# Neutral Current Single Pion Production at High Energies

Hylke Damien
UGent

Promotors:
Natalie Jachowicz
Alexis Nikolakopoulos

15/06/2020

# Chapter 1

# Introduction

## 1.1 A Long time ago in Physics...

### 1.1.1 The idea of Neutrinos

At the start of the 20th century it was thought [1] that beta decay, a radioactive decay in which a nucleus emits an electron, was a 2-body decay: ${}^{A}_{Z}N \rightarrow {}^{A}_{Z+1}N' + e^{-}$. If that is the case we know the energy of the outgoing electron to be $E_e = (m_N - m_{N'})c^2 = E_0$, by energy conservation. Note that the kinetic energy of the nucleus was neglected because of the large mass difference between nucleus and electron. For the rest of this work we set $c = 1$.

In 1914, James Chadwick measured the energy spectrum of the electron [2]. To his surprise he did not observe the expected narrow spectrum around $E_0$ but instead found a continuous spectrum of electron energies ranging all the way from $E_e \approx 0$ to $E_e = E_0$. It seemed that the description of beta decay as a 2-body decay contradicted the law of conservation of energy! Other experiments showed that linear and angular momentum were also apparently not conserved in this reaction. Physicists are wary to throw out conservation laws, so they presumed that the 2-body description of beta decay was flawed.

Wolfgang Pauli proposed a solution to this problem in 1930 [3]. In a letter addressed to "radioactive ladies and gentlemen" he postulated that in beta decay a new electrically neutral particle was emitted: ${}^{A}_{Z}N \rightarrow {}^{A}_{Z+1}N' + e^{-} + \nu$. This particle would account for the missing energy ($E_e + E_\nu = E_0$) and momentum, but was electrically neutral and did not interact via the strong interaction, so it had not been detected yet. At the time Pauli called these particles 'neutrons', but today they are known as neutrinos. Three years later Enrico Fermi [4] made these ideas concrete in his 'theory of beta decay'. From his theory calculations were made for the cross section of a neutrino interacting with matter, through for example $\bar{\nu}_e + p \rightarrow e^{+} + n$. These cross sections were so small that, at the time, all hope of directly observing a neutrino was lost... [5]

### 1.1.2 The Experimentalists Strike Back

As time went on, the realization grew that a small cross section was not a dead-end as long as the neutrino flux was high enough. In 1956 Frederick Reines and Clyde Cowan reported [6] the result of an experiment that used a nuclear reactor as a neutrino source, with a neutrino flux of $10^{13}$ cm$^{-2}$s$^{-1}$ near the reactor (which is huge). The reaction they were looking for was $\bar{\nu}_e + p \rightarrow e^+ + n$. The outgoing positron would annihilate with an electron into two photons, which could be experimentally detected. Furthermore, when the neutron recombined with a nucleus (the experiment used Cadmium as a neutron absorber) it also emitted a photon. So the detection of two photons (from the positron annihilation) followed a few microseconds later by another photon (from the neutron recombination) should be the signature of a neutrino event. Indeed, Reines and Cowan observed a number of those events, and they matched with the low cross section calculated by Fermi's theory. The neutrino had been discovered!

The neutrino that Reines and Cowan observed was actually an antineutrino. At the time it was not known whether there was any distinction between antineutrino and neutrino. In 1958 Raymond Davis Jr. presented evidence [7] that the neutrinos from these nuclear reactions would only interact to form positrons and not electrons. So the neutrinos and antineutrinos seemed to be distinct particles. From now on, we will name them electron (anti)neutrinos, denoted $\nu_e(\bar{\nu}_e)$.

In the early 60s there were the first indications that more neutrino species existed. The recently discovered pion ($\pi$) and muon ($\mu$) were both observed to be decaying with missing energy. Neutrinos were once more the prime suspect, but it was unclear if these should be the same as the electron neutrinos in beta decay. To find an answer Leon Lederman, Melvin Schwartz, and Jack Steinberger studied the decay of pions in a particle collider at BNL [8]. From a theoretical calculation it was known that pions prefer to decay into muons rather than electrons. If the neutrinos produced in the reaction $\pi^+ \rightarrow \mu^+ + \nu$ were of a different kind than the 'electron neutrinos', then they could only interact with a nucleus to form muons. If not, production of electrons should be observed. In their experiments they placed a barrier that stopped the muons formed in the pion decay but was traversable for neutrinos. In the detector, they were looking for the production of muons and electrons and while they found a number of muons, not a single electron was observed. They concluded that this neutrino must be different from the electron neutrino. This was the discovery of the muon neutrino $\nu_\mu$.

The discovery of another electron-like particle in 1975 [9], the tau particle, seemed to indicate the existence of a third neutrino species. It was not until 2000 that the DONUT experiment at Fermilab first detected this tau neutrino $\nu_\tau$ [10].

### 1.1.3 The Standard Model is born

While the experimental side of particle physics was discovering these neutrinos, the theorists were not just sitting around. By the mid-1970s, work on a theory of particle physics that could describe the fundamental particles and forces (except for gravity) was completed. This theory, the Standard Model, is the model we use to this day and has been hugely successful when its calculations are put to the test [11].

The Standard Model describes three classes of particles: elementary bosons, quarks and leptons. These latter two describe the 'matter' in the Universe. Both the leptons and the quarks are divided into particle pairs with similar behavior called generations. Quarks combine into composite particles known as hadrons, usually divided into mesons (consisting of a quark and an antiquark) and baryons (generally containing 3 quarks). For example, the first generation of quarks consists of the up and down quark, which are the constituent particles in the familiar nucleons, proton and neutron (baryons), but can form other particles such as the pion. The heavier generations in the quark sector are the charm and strange quark (2nd generation) and the top and bottom quark (3rd generation).

In the leptonic sector, the most well-known particle is the negatively charged electron and its partner for the first generation is the electron neutrino. For the rest of the leptons we find the familiar muon and muon neutrino and the tau and tau neutrino. The Standard Model also includes their respective antiparticles.

If the quarks and leptons describe the 'matter', then the interactions between the matter particles is described by the exchange of bosons. The elementary bosons are divided into scalar bosons and gauge bosons. We know of only one scalar boson, the Higgs boson, which is related to how elementary particles get mass. The four elementary bosons each representing a fundamental interaction ('forces') : the photon (electromagnetic interaction), the gluons (strong interaction) and the W and Z bosons (weak interaction). This weak interaction lies at the heart of reactions like beta decay and is the modern version of Fermi's interaction.

The Standard Model has proven itself to be a powerful theory, giving us a lot of predictions that turned out to be correct. But we know that the Standard Model is incomplete, as one of its assumptions turned out to be incorrect! And that flaw lurking inside the Standard Model turned out to be caused by neutrinos...

To summarize, we needed a particle to account for energy loss in beta decay, so the neutrino was proposed. This neutrino has been observed and, as of today, fits nicely in the Standard Model. There are 3 'flavours' of them (electron, muon and tau), they interact only through the weak interaction and according to the Standard Model they have zero mass. Remember that last one.

## 1.2 Of Neutrino Oscillations and Mass

### 1.2.1 Solar Neutrino Problem

To see where neutrino physics comes into disagreement with the Standard Model, we have to take a step back in time. Developments in nuclear physics in the first half of the 20th century made it possible to construct a model for the nuclear reactions inside the Sun [12]. This Standard Solar Model (SSM) claimed that the Sun is primarily fueled by the pp-chain reaction: $4p \rightarrow {}^4He + 2e^+ + 2\nu_e + 2\gamma$. The model, combined with properties of the Sun that had already been measured, produced a first estimate of the solar neutrino flux arriving on Earth [13].

In the early 1960s Raymond Davis, together with John Bahcall, carried out the Homestake Experiment, measuring this flux for the first time. They detected about a third of the amount of neutrinos expected by the SSM. This discrepancy would be known as the Solar Neutrino Problem. Early efforts to solve it focused on the SSM, claiming that some assumptions made in the theory (such as internal temperature of the Sun) were wrong. These efforts would prove to be futile. It was found that while the neutrino flux was not as expected, the neutrino energy spectrum did match with the observations. Other experiments were able to measure and confirm that the internal temperature used in the SSM was right. Finally, in atmospheric neutrinos, a similar disagreement between theory and experiment was found.

The solution to this problem was proposed as far back as 1957 but was only conclusively identified as the correct one in 2001. So what was it? Neutrino oscillations!

### 1.2.2 Neutrino oscillations

We'll describe the theory of neutrino oscillations first for two neutrino flavours, and then we generalize, look at the experimental evidence and the impact that neutrino oscillations have on the Standard Model.

The idea of neutrino oscillations, first proposed by Pontecorvo [14], is that the neutrino 'flavour states' ($\nu_e$, $\nu_\mu$, $\nu_\tau$) which are the eigenstates in which the neutrinos are produced, don't have well-defined masses, because they don't match up with the so-called 'mass states' ($\nu_1$, $\nu_2$, $\nu_3$), which are neutrino states with a well-defined mass. Instead, the flavour states exist as a quantum superposition of the mass states. After production, the neutrino travels to the detector, and the mass states, having different momenta because of their differing masses, acquire a phase difference. When the mass states recombine at the detector, these phase differences change the composition of the original neutrino. By this change of composition a neutrino created as an electron neutrino that travels a certain distance could be detected as a muon neutrino.

We'll describe this idea a bit more mathematically, using 2 flavour states ($\nu_e$, $\nu_\mu$) and 2 mass states ($\nu_1$, $\nu_2$). This will make the calculations and conclusions easier and the extension to 3 states is fairly straightforward. The relation

between these states is described as

$$\begin{bmatrix} \nu_e \\ \nu_\mu \end{bmatrix} = U \begin{bmatrix} \nu_1 \\ \nu_2 \end{bmatrix}$$

with the mixing matrix U given by

$$\begin{bmatrix} U_{e1} & U_{e2} \\ U_{\mu 1} & U_{\mu 2} \end{bmatrix} = \begin{bmatrix} \cos(\theta) & \sin(\theta) \\ -\sin(\theta) & \cos(\theta) \end{bmatrix}$$

where $\theta$ is the mixing angle. Let's say in a reaction (in the sun for instance) an electron neutrino is produced:

$$|\nu(t=0)\rangle = |\nu_e\rangle = \cos(\theta)\,|\nu_1\rangle + \sin(\theta)\,|\nu_2\rangle$$

While this neutrino is produced with a certain fixed energy $E$, it has different momenta for each of the mass states, because of the difference in their masses. The phase of the mass states is therefore slightly different:

$$\phi_i = Et - p_i L = Et - \sqrt{E^2 - m_i^2}L \approx Et - EL + \frac{m_i^2 L}{2E}$$

The initial state evolves, after a time t, into:

$$|\nu(t)\rangle = \cos(\theta)e^{-i\phi_1}\,|\nu_1\rangle + \sin(\theta)e^{-i\phi_2}\,|\nu_2\rangle$$

This phase difference can cause the electron neutrino to be detected as a muon neutrino. The chance of that happening, after a time t, is calculated as:

$$P(\nu_e \to \nu_\mu; t) = |\,\langle\nu_\mu|\nu(t)\rangle\,|^2 = |\,-\sin(\theta)\,\langle\nu_1|\nu(t)\rangle + \cos(\theta)\,\langle\nu_2|\nu(t)\rangle\,|^2$$

$$= \cos^2(\theta)\sin^2(\theta)|\,-e^{-i\phi_1} + e^{-i\phi_2}|^2 = 2\cos^2(\theta)\sin^2(\theta)\,(1-\cos(\phi_2-\phi_1))$$

$$= 2\sin^2(2\theta)\sin^2\left[\frac{\Delta m^2}{4E}L\right]$$

where $\Delta m^2 = m_2^2 - m_1^2$. Let us look at this formula for a moment. First of all there are 2 parameters in this expression that are unknown a priori: the mixing angle $\theta$ and the squared mass difference $\Delta m^2$. These parameters would have to be determined by experiments. Furthermore, these oscillations depend on the energy of the produced neutrino and on the distance it travelled. It is important to stress that while distance is easily measured, the neutrino energy is not. Remember that neutrinos can only be detected indirectly by their interactions with other particles that we can directly detect. Reconstructing the energy of a neutrino is thus of a great importance if we want to measure the 2 parameters correctly. Keep that in mind.

So with this theory of neutrino oscillations, we can go back to the Solar problem. In the experiment of Davis and Bahcall only electron neutrinos were detected, as that was the only species that would be produced in the Sun. But if we take neutrino oscillations into account, a number of these original

electron neutrinos could oscillate into other neutrino species. So the theory of neutrino oscillations predicted that the expected neutrino flux would be found when taking into account all neutrino species. Indeed, new experiments were set up and did confirm this. Numerous experiments followed that confirmed that neutrino oscillations were the mechanism behind the Solar problem. Eventually, this was rewarded by a Nobel Prize in Physics to Takaaki Kajita and Arthur B. McDonald for their work in the discovery of neutrino oscillations.

Up until now we have worked out the oscillations assuming only two neutrino species, but we can extend it. For three flavour and mass states, the analysis is analogous but a bit more complicated. Now the mixing matrix is 3-dimensional:

$$U = \begin{bmatrix} U_{e1} & U_{e2} & U_{e3} \\ U_{\mu 1} & U_{\mu 2} & U_{\mu 3} \\ U_{\tau 1} & U_{\tau 2} & U_{\tau 3} \end{bmatrix}$$

This matrix is the Pontecorvo–Maki–Nakagawa–Sakata (PMNS) matrix. It can be expressed in terms of 3 mixing angles ($\theta_{12}$, $\theta_{23}$, $\theta_{13}$) and a CP violating phase $\delta$,

$$U = \begin{bmatrix} 1 & 0 & 0 \\ 0 & \cos(\theta_{23}) & \sin(\theta_{23}) \\ 0 & -\sin(\theta_{23}) & \cos(\theta_{23}) \end{bmatrix} \begin{bmatrix} \cos(\theta_{13}) & 0 & \sin(\theta_{13})e^{-i\delta} \\ 0 & 1 & 0 \\ -\sin(\theta_{13})e^{i\delta} & 0 & \cos(\theta_{13}) \end{bmatrix} \begin{bmatrix} \cos(\theta_{12}) & \sin(\theta_{12}) & 0 \\ -\sin(\theta_{12}) & \cos(\theta_{12}) & 0 \\ 0 & 0 & 1 \end{bmatrix}$$

Together with the 3 mass differences these are the oscillation parameters that neutrino experiments are trying to constrain.

To give an idea of where we are today, these are a set of values of the oscillation parameters from [15],

$$\sin^2(\theta_{12}) = 0.307^{+0.013}_{-0.012}$$

$$\sin^2(\theta_{13}) = (2.18^{+0.07}_{-0.07})10^{-2}$$

$$\sin^2(\theta_{23}) = 0.512^{+0.019}_{-0.022}$$

$$\Delta m^2_{12} = (7.53 \pm 0.18)10^{-5} eV^2$$

$$|\Delta m^2_{13}| = (2.44 \pm 0.03)10^{-3} eV^2$$

As this is a hot field of research these values are constantly being refined and challenged, but it is interesting to get an idea of their order of magnitude.

So a deficit in the number of observed solar neutrinos led us to the neutrino oscillations, but why are these so interesting? Remember that one of the parameters in the oscillation is the squared mass difference $\Delta m^2$. That quantity has to be non-zero, or there would be no oscillations. But if we turn back to the Standard Model, we assumed massless neutrinos and thus $\Delta m^2 = 0$. So neutrino oscillations are in conflict with the Standard Model, as they require neutrinos to be massive! We know that neutrino oscillations do happen, so they give us a tantalizing hint at physics beyond the Standard Model (BSM).

## 1.3 Current Neutrino Research

### 1.3.1 Open Neutrino Problems

It is clear that a thorough understanding of neutrino oscillations is of high importance if we want to unravel the hints at BSM physics. Today there are still a number of unknowns that we have to find out. First of all there is the question of the nature of neutrinos (Majorana or Dirac particle) and the absolute mass scale. Though interesting problems, they have no solution to be found in neutrino oscillations, so we will not discuss them here.

Neutrino mass ordering is the question of which neutrino mass state is the heaviest. We know that $m_2 > m_1$ but we don't know if $m_3$ is larger than them (normal hierarchy) or smaller (inverted hierarchy). A more precise determination of oscillation parameters could give us an idea which mass ordering is correct.

In recent years, anomalies have been found in short baseline oscillation experiments, such as the LSND[16] and the MiniBooNE [17]experiment. In those experiments a deficit of neutrinos was observed. This sparked the idea of a 4th generation of neutrino, the sterile neutrino, that cannot interact with other particles. By oscillating into this 4th state which cannot be detected the deficit could be explained. More exact measurements could prove or disprove this idea.

The parameter $\delta$, the Dirac CP-violating phase has also not been measured with high precision yet.

All these open problems require very precise measurements of the oscillation parameters, an endeavour which is interesting on its own. In addition there is theoretical interest in the structure of the PMNS matrix, for which we need to know the exact value of the matrix elements.

### 1.3.2 Wanted: Neutrino-nucleus cross section

The group of experiments that we are mainly focused on in this work consist of the accelerator-based neutrino experiments. In these experiments, a proton beam in an accelerator is collided with a mesonic target that decays into neutrinos. The advantage of using accelerators to produce neutrinos is that a high neutrino flux can be obtained by focusing the produced mesons, with the use of magnets, in the direction of the detector. The accelerated beam can also be changed to produce other flavours or distributions of energies in the neutrinos and the length of the so-called 'decay tunnel' can be optimized to obtain a specific neutrino flavour. Examples of such experiments are CNGS, T2K, DUNE, MiniBooNE, MINER$\nu$A, ...

One of the main sources of systematic errors in these high-precision measurements from accelerator-based neutrino experiments is the neutrino-nucleus cross section [18] [19]. As we have pointed out earlier, the neutrino energy is one of the variables crucial for an oscillation experiment. Neutrinos are only indirectly detected so we need to reconstruct their energy, a process made more difficult by the interactions going on inside a nucleus. A neutrino that passes

through a nucleus doesn't only produce leptons through $\nu_e + n \to e^- + p$, the charged current (CC) quasi-elastic (QE) channel. There is a whole spectrum of possible interactions between the neutrino and nucleus. These interactions take away part of the observed neutrino flux or can produce signals that we mistake for the straightforward neutrino signal. So in order to reconstruct the neutrino energy in a correct way, a good knowledge of the neutrino-nucleus cross section is required.

A lot of theoretical effort is currently put into better models for the neutrino-nucleus cross section. One of the areas that needs work is the neutrino-induced pion production as many current and future experiments, such as MINER$\nu$A, NOvA and DUNE, are right in the region where meson production processes become important.[20]

### 1.3.3 Single Pion Production

Let us quickly review some properties of pions [11]. Pions are mesons, composite particles consisting of a quark and an antiquark, and there are three types: $\pi^+ = u\bar{d}$, $\pi^0 = u\bar{u}/d\bar{d}$, $\pi^- = d\bar{u}$. Pions are the lightest mesons with masses of 139 MeV for the charged pions and 134 MeV for the neutral pion.

The dominant meson production channel is single pion production (SPP),

$$l + N \to l' + N' + \pi$$

with $l$ and $l'$ being leptons, $N$ and $N'$ nuclei.

The cross section for pion production processes become relevant for $E_\nu > 0.5$ GeV, and becomes one of the main reaction mechanisms at multiple GeV energies. Pion production is an important background to $\nu_\mu$ disappearance experiments. The produced charged pion can be absorbed by a nucleus and mimic the signal of the quasi-elastic channel, $\nu_\mu + n \to \mu^- + p$, in the detector. Similarly the signal of a neutral pion is the main background in $\nu_e$ appearance experiments. If the pion production model is in bad agreement with the data, the error propagates to the neutrino energy used to determine the oscillation parameters. [20]

As a step towards single pion production off a nucleus, we start with SPP at the nucleon level. A number of good low-energy models exist, describing the process up through $\pi N$-invariant mass $W \lesssim 1.4$ GeV. But these models break down in the high-energy regions. In this thesis we study a description of pion production at higher W, using Regge phenomenology. Earlier work making use of the Regge approach, such as [20], has been focusing on Reggeizing terms from a Chiral Perturbation Theory Background model. This has had a fair amount of success in its calculations, but it is somewhat limited by the ChPT backgrounds.

In this work we start from a Born term model, which we extend to high energies using the Regge approach. An advantage of such an approach is that most of the parameters are constrained by the low energy Born term model. The goal is to describe neutrino-induced pion production (later called neutrinoproduction) but an important step along that road is having a working description

of the vector current part of pion production. This is exactly what we have in electron-induced pion production (electroproduction), so we focus on working out that first and then we will extend it to axial currents.

We begin with the model by Laget, Guidal and Vanderhaegen [21] for photon-induced pion production (photoproduction), which is a first benchmark on the way to electroproduction. This is useful as photoproduction is the $Q^2 = 0$ limit of electroproduction. For an extension to $Q^2 > 0$, we will look at the work of Kaskulov and Mosel [22] [23] and later refinements by Vranckx and Ryckebusch [24].

## 1.4 Outline of thesis

In chapter 2, we will work out the relevant kinematics for the pion production processes. That is followed by an introduction to Regge theory and an explanation of the procedure of reggeization that we will use. Then we will show the results of our model. Chapter 4 handles photoproduction, which is a first check for our model. Then we extend it to electroproduction in Chapter 5 and discuss the several ways in which the dependence on $Q^2 \neq 0$ can be implemented. Finally we go the last step and test our model for neutrino-induced pion production in Chapter 6.

# Chapter 2

# Kinematics

## 2.1 Definition of Kinematic variables

Consider the process:

$$l(k) + N(p) \rightarrow l'(k') + N'(p') + \pi(k_\pi)$$

In the LAB system the four-momenta of the initial lepton, final lepton, initial nucleon, final nucleon and pion are given by $k^\mu = (E_l, 0, 0, |\mathbf{k}|)$, $k'^\mu = (E'_l, \mathbf{k}')$, $p^\mu = (M, 0, 0, 0)$, $p'^\mu = (E'_N, \mathbf{p}')$, $k_\pi = (E_\pi, \mathbf{k}_\pi)$, with $M$ the nucleon mass.

Furthermore the boson exchanged in this reaction, either a photon or a W/Z boson, has four-momentum $Q^\mu$. Somewhat confusingly the variable $Q^2$ is defined as $Q^2 = -Q^\mu Q_\mu$.

For the hadronic subreaction $B(Q) + N(p) \rightarrow N'(p') + \pi(k_\pi)$, where $B$ is the exchanged boson, we will additionally define the Mandelstam variables and their corresponding four-momenta: $q^\mu \equiv p_t^\mu = (Q - k_\pi)^\mu$ and $t = (Q - k_\pi)^2$, $p_s^\mu = (Q + p)^\mu$ and $s = (Q + p)^2$, $p_u^\mu = (Q - p')^\mu$ and $u = (Q - p')^2$. When we speak of t/s/u-channel processes we mean those processes where the exchanged particle in the subreaction has momentum $p_t/p_s/p_u$. Another variable often used when describing the kinematics of these sub-processes is the invariant mass $W = \sqrt{s} = Q^{*0} + E_N^* = E_{N'}^* + E_\pi^*$ (where the star denotes the Center of Mass system).

## 2.2 General Expression for Cross section

The general expression for the interaction cross section for the process above is [26][25]

$$\sigma = \int \frac{1}{\Phi} |\mathcal{M}|^2 (2\pi)^4 \delta^4(k + p - k' - k_\pi - p') \frac{d^3\mathbf{k}'}{(2\pi)^3 2E'_l} \frac{d^3\mathbf{p}'}{(2\pi)^3 2E'_N} \frac{d^3\mathbf{k}_\pi}{(2\pi)^3 2E_\pi}$$

The flux factor $\Phi$ is defined as:

$$\Phi = 4\sqrt{(p \cdot k)^2 - m_l^2 M^2}$$

where $m_l$ is the lepton mass. The flux factor is a Lorentz-invariant quantity so it can be reformulated in the LAB-system as:

$$\Phi = 4M\sqrt{E_l^2 - m_l^2} = 4M|\mathbf{k}|$$

We will first work out this cross section in the case of neutrinoproduction, following the work done in [27]. We refer to that paper for more detail. Having derived that, we will show it is straightforward to reduce to the cross section for electroproduction and photoproduction.

## 2.3 Kinematics of Neutrinoproduction

As the interactions of the reaction are completely contained in the matrix element we will work that out first before plugging it back in the cross section

In the case of charged current interactions with an incident neutrino, the matrix element is of the form:

$$\begin{aligned}\mathcal{M} = &\left(\frac{g}{2\sqrt{2}}\right)^2 \bar{u}_l(k')\gamma_\alpha(1-\gamma_5)u_\nu(k)\left(\frac{i}{Q^2 - M_W^2}\right)\left(-g^{\alpha\beta} + \frac{Q^\alpha Q^\beta}{M_W^2}\right) \\ &\langle N'(p',s'), \pi(k_\pi)|J^\nu(0)|N(p,s)\rangle \\ &= i\frac{G_F}{\sqrt{2}} u_l(k')\gamma_\alpha(1-\gamma_5)u_\nu(k)\,\langle N'(p',s'), \pi(k_\pi)|J^\nu(0)|N(p,s)\rangle\end{aligned}$$

where we approximated $|Q^2| << M_W^2$ and defining $\frac{G_F}{\sqrt{2}} = \frac{g^2}{8M_W^2}$. In the spin-averaged squared matrix element

$$|\mathcal{M}|^2 = \frac{G_F^2}{2} L'_{\mu\nu}\mathcal{H}^{\mu\nu}$$

we introduced the leptonic tensor $L'_{\mu\nu}$

$$L'_{\mu\nu} = \sum_{spin}[\bar{u}_l(k')\gamma_\mu(1-\gamma_5)u_\nu(k)]^\dagger[\bar{u}_l(k')\gamma_\nu(1-\gamma_5)u_\nu(k)]$$

and the hadronic tensor $\mathcal{H}^{\mu\nu}$

$$\mathcal{H}^{\mu\nu} = \frac{1}{2}\sum_{s,s'}\langle N'(p',s'), \pi(k_\pi)|J^\mu(0)|N(p,s)\rangle\,\langle N'(p',s'), \pi(k_\pi)|J^\nu(0)|N(p,s)\rangle^*$$

with $J^\mu(0)$ being the hadronic current operator.

We can work out the lepton tensor using the well-known trace technique[26]:

$$\begin{aligned}
L'_{\mu\nu} &= Tr\left(\sum_{spin}[u_\nu(k)\bar{u}_\nu(k)\gamma_\mu(1-\gamma_5)u_l(k')\bar{u}_l(k')\gamma_\nu(1-\gamma_5)]\right) \\
&= Tr[(\not{k}+m_\nu)\gamma_\mu(1-\gamma_5)(\not{k}'+m_l)\gamma_\nu(1-\gamma_5)] \\
&= 2Tr[k^\alpha\gamma_\alpha\gamma_\mu(1-\gamma_5)k'^\beta\gamma_\beta\gamma_\nu] \\
&= 8(g_{\alpha\mu}g_{\beta\nu}-g_{\alpha\beta}g_{\mu\nu}+g_{\alpha\nu}g_{\beta\mu}-i\epsilon_{\alpha\mu\beta\nu})k^\alpha k'^\beta \\
&= 8[k_\mu k'_\nu - g_{\mu\nu}(k\cdot k')+k_\nu k'_\mu]+8i\epsilon_{\mu\nu\alpha\beta}k^\alpha k'^\beta
\end{aligned}$$

The first term in the final expression is the symmetric part of the lepton tensor denoted as $8L^S_{\alpha\beta}$ and the second term is the antisymmetric part $8iL^a_{\alpha\beta}$. In the case of an incident antineutrino the antisymmetric part changes sign. The hadronic tensor is more complex as it contains the strong interactions inside the nucleons. Nevertheless it is of great importance, as the hadronic current is the model-dependent factor in this cross section.

Now we plug in the squared matrix element in the cross section

$$\sigma = \frac{G_F^2}{2}\frac{1}{4\pi^2}\frac{1}{4M|\mathbf{k}|}\frac{1}{4}\int\frac{d^3\mathbf{k}'}{E'_l}\frac{d^3\mathbf{k}_\pi}{E_\pi}\frac{d^3\mathbf{p'_N}}{(2\pi)^3 2E'_N}\delta^4(k+p-k'-k_\pi-p')L'_{\mu\nu}\mathcal{H}^{\mu\nu}$$

Both the lepton and hadron tensor are usually redefined as

$$L_{\mu\nu}(k,k') = \frac{1}{8}L'_{\mu\nu} = [k_\mu k'_\nu - g_{\mu\nu}(k\cdot k')+k_\nu k'_\mu]+i\epsilon_{\mu\nu\alpha\beta}k^\alpha k'^\beta$$

$$W^{\mu\nu}(Q,p,k_\pi) = \frac{1}{4M}\int\frac{d^3\mathbf{p}'}{(2\pi)^3 2E'_N}\delta^4(k+p-k'-k_\pi-p')\mathcal{H}^{\mu\nu}(p,p',k_\pi)$$

in order to get

$$\sigma = \frac{G_F^2}{4\pi^2|\mathbf{k}|}\int\frac{d^3\mathbf{k}'}{E'_l}\frac{d^3\mathbf{k}_\pi}{E_\pi}L_{\mu\nu}W^{\mu\nu}$$

The quantity $L_{\mu\nu}W^{\mu\nu}$ is Lorentz-invariant so $L_{\mu\nu}(k,k')W^{\mu\nu}(Q,p,k_\pi) = L_{\mu\nu}(\Lambda k,\Lambda k')W^{\mu\nu}(\Lambda Q,\Lambda p,\Lambda k_\pi)$. We chose the Lorentz transformation $\Lambda$ so that the transformed momenta correspond to those in the center-of-mass system of the pion-nucleon system. In the new coordinate system, where we denote the vector $\mathbf{a}$ as $\mathbf{a}^*$, $\mathbf{Q}^*$ lies along the positive z-axis and the positive y-axis is perpendicular to the plane constructed by the vectors $\mathbf{k}^*$ and $\mathbf{k}'^*$. In the cross section we will change variables $\mathbf{k}_\pi$ to ${\mathbf{k}_\pi}^*$.

Three observations can be made about these new four-momenta. First none of them are dependent on $\phi'$ so the integral over $\phi'$ gives a factor $2\pi$. Furthermore the second spatial components of $\mathbf{k}^*$ and $\mathbf{k}'^*$ are zero. This has consequences for the non-diagonal components of the lepton tensor. The $L_{a2}$ components ($a = 0,1,3$) are now antisymmetric ($L_{a2} = -L_{2a}$), while the other components are symmetric. Finally both $\mathbf{Q}^*$ and $\mathbf{p}^*$ have zero first and second spatial components (as they lie completely along the new z-axis).

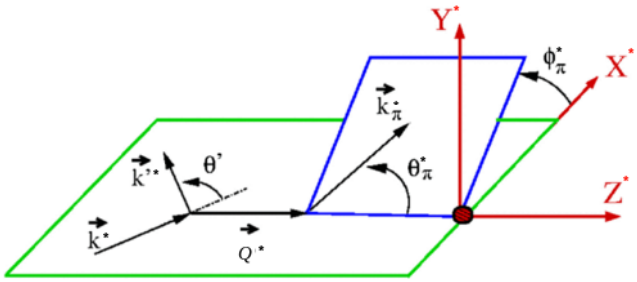


Figure 2.1: Illustration of the different momentum vectors in the new coordinate frame. Original image is from [27] and has been edited to fit our convention.

After doing the integration over $d^3p'^*$ (in the hadron tensor) using the delta function, the differential cross section can be rewritten as

$$\frac{d^5\sigma}{d\Omega' dE'_l d\Omega^*_\pi} = \frac{G_F^2}{256\pi^5}\frac{|\mathbf{k}'|}{M|\mathbf{k}|}\int \frac{|\mathbf{k}^*_\pi|^2 d|\mathbf{k}^*_\pi|}{E^*_\pi E'^*_N} L_{\mu\nu}\mathcal{H}^{\mu\nu}\delta(W - E'^*_N - E^*_\pi)$$

We can express the delta function as $\delta(f(|\mathbf{k}_\pi|)$ which is 0 at $|\mathbf{k}^*_\pi|$. By using the delta function property: $\delta(f(x)) = \frac{\delta(x-x_0)}{|f'(x_0)|}$ if $f(x_0) = 0$, the integral works out as

$$\int \frac{|\mathbf{k}^*_\pi|^2 d|\mathbf{k}^*_\pi|}{E^*_\pi E'^*_N}\delta(W - \sqrt{M^2 + |\mathbf{k}^*_\pi|^2} - \sqrt{m_\pi^2 + |\mathbf{k}^*_\pi|^2}) = \frac{|\mathbf{k}^*_\pi|}{W}$$

and we arrive at

$$\frac{d^5\sigma}{d\Omega' dE'_l d\Omega^*_\pi} = \frac{G_F^2|\mathbf{k}^*_\pi|}{256\pi^5 MW}\frac{|\mathbf{k}'|}{|\mathbf{k}|}L_{\mu\nu}\mathcal{H}^{\mu\nu}$$

Before we go on a few remarks are in order.

The differential cross section can be expressed differently by a change of variables from $(\Omega', E'_l, \Omega^*_\pi)$ to $(Q^2, W, \Omega^*_\pi)$, where we also did the trivial integration over $\phi'$. The Jacobian for this change is easy to compute knowing that $Q^2 = 2|\mathbf{k}||\mathbf{k}'|(1 - \cos\theta')$ and

$$W = \sqrt{(Q+p)^2} = \sqrt{-2|\mathbf{k}||\mathbf{k}'|(1-\cos\theta') + 2M(|\mathbf{k}| - |\mathbf{k}'|) + M^2}$$

In the end we obtain

$$\frac{d^4\sigma}{dQ^2 dW d\Omega^*_\pi} = \frac{G_F^2|\mathbf{k}^*_\pi|}{256\pi^4 M^2|\mathbf{k}|^2}L_{\mu\nu}\mathcal{H}^{\mu\nu}$$

In the cross section the factor $|\mathbf{k}^*_\pi|$ appears. Making use of the identity

$$W = E^*_\pi + E'^*_N = \sqrt{m_\pi^2 + |\mathbf{k}^*_\pi|^2} + \sqrt{M^2 + |\mathbf{k}^*_\pi|^2}$$

we can calculate $|\mathbf{k}^*_\pi|$ to be

$$|\mathbf{k}^*_\pi| = \frac{\sqrt{(W^2 + M^2 - m_\pi^2)^2 - 4W^2M^2}}{2W}$$

The cross section we derived is for the case of a charged current with an incident neutrino. For the incident antineutrino, the only difference is the sign change of the antisymmetric part of the leptonic tensor. In the case of a neutral current, there is an extra factor 1/4, as the matrix element for the neutral current is:

$$\mathcal{M} = \left(\frac{g}{4\cos\theta_W}\right)^2 \bar{u}_\nu(k')\gamma_\alpha(1-\gamma_5)u_\nu(k)\left(\frac{i}{Q^2-M_Z^2}\right)\left(-g^{\alpha\beta}+\frac{Q^\alpha Q^\beta}{M_Z^2}\right)$$
$$\langle N'(p',s'),\pi(k_\pi)|J^\nu(0)|N(p,s)\rangle$$

and $M_Z^2\cos^2\theta_W = M_W^2$.

### 2.3.1 Angular dependence of hadron tensor

It is possible to isolate the $\phi_\pi^*$-dependence of the differential cross section. Knowing that the four-momentum of the pion is

$$k_\pi^{*\mu} = (E_\pi^*, |\mathbf{k}_\pi^*|\sin(\theta_\pi^*)\cos(\phi_\pi^*), |\mathbf{k}_\pi^*|\sin(\theta_\pi^*)\sin(\phi_\pi^*), |\mathbf{k}_\pi^*|\cos(\theta_\pi^*))$$

we consider a rotation $\hat{R}$ that rotates over an angle $\phi_\pi^*$ in the xy-plane:

$$\hat{R} = \begin{pmatrix} 1 & 0 & 0 & 0 \\ 0 & \cos(\phi_\pi^*) & -\sin(\phi_\pi^*) & 0 \\ 0 & \sin(\phi_\pi^*) & \cos(\phi_\pi^*) & 0 \\ 0 & 0 & 0 & 1 \end{pmatrix}$$

Using the inverse rotation on the pion four-momentum we get:

$$(\hat{R}^{-1}k_\pi^*)^\mu = (E_\pi^*, |\mathbf{k}_\pi^*|\sin(\theta_\pi^*), 0, |\mathbf{k}_\pi^*|\cos(\theta_\pi^*))$$

while $p^*$ and $Q^*$ are invariant under the same rotation, as their first and second spatial components are zero. Now, because of the tensorial nature of the hadron tensor we can isolate its $\phi_\pi^*$-dependence making use of the rotation

$$\begin{aligned} W^{\mu\nu}(Q^*,p^*,k_\pi^*) &= W^{\mu\nu}(\hat{R}\hat{R}^{-1}Q^*, \hat{R}\hat{R}^{-1}p^*, \hat{R}\hat{R}^{-1}k_\pi^*) \\ &= \hat{R}_\alpha^\mu\hat{R}_\beta^\nu W^{\alpha\beta}(\hat{R}^{-1}Q^*, \hat{R}^{-1}p^*, \hat{R}^{-1}k_\pi^*) \\ &= \hat{R}_\alpha^\mu\hat{R}_\beta^\nu W^{\alpha\beta}(Q^*, p^*, \hat{R}^{-1}k_\pi^*) \\ &\equiv \hat{R}_\alpha^\mu\hat{R}_\beta^\nu \widetilde{W}^{\alpha\beta} \end{aligned}$$

$\widetilde{W}$ is the hadron tensor evaluated at $\phi_\pi^* = 0$ and therefore has no $\phi_\pi^*$-dependence. The dependence on $\phi_\pi^*$ is solely contained in $\hat{R}$. We have effectively written the original hadron tensor as rotation of the hadron tensor in the $x,z$-plane. By performing the rotations explicitly, we can write out $W^{\mu\nu}$ in terms of $\widetilde{W}^{\mu\nu}$. Grouping together the $\phi_\pi^*$-dependencies we can express the cross section as:

$$\frac{d^5\sigma}{d\Omega' dE' d\Omega_\pi^*} = \frac{|\mathbf{k}'|}{|\mathbf{k}|}\frac{G_F^2}{4\pi^2}\left(A^* + B^*\cos\phi_\pi^* + C^*\cos 2\phi_\pi^* + D^*\sin\phi_\pi^* + E^*\sin 2\phi_\pi^*\right)$$

with the five angular structure functions defined as

$$A^* = \int \frac{|\mathbf{k}_\pi^*|^2 d|\mathbf{k}_\pi^*|}{E_\pi^*} \left[ L_{00}\widetilde{W}_{(s)}^{00} + 2L_{03}\widetilde{W}_{(s)}^{03} + L_{33}\widetilde{W}_{(s)}^{33} + \frac{1}{2}(L_{11}+L_{22})\left(\widetilde{W}_{(s)}^{11} + \widetilde{W}_{(s)}^{22}\right) + 2iL_{12}\widetilde{W}_{(a)}^{12} \right]$$

$$B^* = \int \frac{|\mathbf{k}_\pi^*|^2 d|\mathbf{k}_\pi^*|}{E_\pi^*} 2\left[ L_{01}\widetilde{W}_{(s)}^{01} + L_{13}\widetilde{W}_{(s)}^{13} + iL_{02}\widetilde{W}_{(a)}^{02} + iL_{23}\widetilde{W}_{(a)}^{23} \right]$$

$$C^* = \int \frac{|\mathbf{k}_\pi^*|^2 d|\mathbf{k}_\pi^*|}{E_\pi^*} \frac{1}{2}\left[ (L_{11}-L_{22})\left(\widetilde{W}_{(s)}^{11} - \widetilde{W}_{(s)}^{22}\right) \right]$$

$$D^* = \int \frac{|\mathbf{k}_\pi^*|^2 d|\mathbf{k}_\pi^*|}{E_\pi^*} 2\left[ -L_{01}\widetilde{W}_{(s)}^{02} - L_{13}\widetilde{W}_{(s)}^{23} + iL_{02}\widetilde{W}_{(a)}^{01} + iL_{23}\widetilde{W}_{(a)}^{13} \right]$$

$$E^* = \int \frac{|\mathbf{k}_\pi^*|^2 d|\mathbf{k}_\pi^*|}{E_\pi^*} \left[ (L_{22}-L_{11})\widetilde{W}_{(s)}^{12} \right]$$

where we split the reduced hadron tensor into symmetric and antisymmetric parts: $\widetilde{W}^{\mu\nu} = \widetilde{W}_{(s)}^{\mu\nu} + i\widetilde{W}_{(a)}^{\mu\nu}$.

Note that when we are considering cross sections integrated over $\phi_\pi^*$, none of the angular factors contribute except for $A^*$.

The problem of calculating the cross section has been reduced to calculating the components of the hadron tensor. We can rewrite the tensor $\mathcal{H}^{\mu\nu}$ to the form that is most useful for our purposes, using the trace method again:

$$\mathcal{H}^{\mu\nu} = \frac{1}{2} Tr\left[ (\not{p}'^* + M)\mathcal{O}^\mu (\not{p}^* + M)\gamma^0 \mathcal{O}^{\nu\dagger}\gamma^0 \right]$$

In this work we will look at specific choices for the current operator $\mathcal{O}^\mu$ to try to describe the neutrino-induced pion production process.

## 2.4 Kinematics of Electroproduction

We will now use the general expressions derived for the neutrino case and specify them in the case of electrons. The matrix element for the electroproduction reaction is given by

$$\mathcal{M} = \frac{e^2}{Q^2}\bar{u}(k')\gamma_\mu u(k) < p'k_\pi |V^\mu| p >$$

Similar to the neutrino case one gets

$$\sum |\mathcal{M}|^2 = \frac{2e^4}{Q^4}\frac{1}{2} L_{\mu\nu} W^{\mu\nu}$$

with $L_{\mu\nu}$ the Lepton tensor and $W^{\mu\nu}$ the hadron tensor. Working out the lepton tensor (and absorbing the extra factor $\frac{1}{2}$ in its definition)

$$L_{\mu\nu} = \frac{1}{4}\sum_{spin} [\bar{u}(k')\gamma_\mu u(k)]^\dagger [\bar{u}(k')\gamma_\nu u(k)]$$

is completely analogous to the neutrino-induced lepton tensor without the antisymmetric part:

$$L_{\mu\nu} = k_\mu k'_\nu - g_{\mu\nu}(k \cdot k') + k_\nu k'_\mu + g_{\mu\nu} m_l^2 = k_\mu k'_\nu + k_\nu k'_\mu - \frac{1}{2} g_{\mu\nu} Q^2$$

Analogous to the previous section we can go to the pion-nucleon system center of mass frame and separate the $\phi_\pi^*$-dependence from the hadron tensor and get the same angular factors. Some simplifications can be made in this case. The lepton tensor has no antisymmetric part so the factors $L_{a2} = 0$ for $a = 0, 1, 3$ (remember that $k$ and $k'$ have a second spatial component that is zero). Now we are only left with symmetric components of the lepton and hadron tensor.

From $\widetilde{W}^{\alpha\beta} \equiv W^{\alpha\beta}(Q^*, p^*, \hat{R}^{-1} k_\pi^*)$ and the fact that none of those hadronic four vectors $(Q^*, p^*, \hat{R}^{-1} k_\pi^*)$ have a second spatial component, we can conclude that for the symmetric hadron tensor: $W^{02} = W^{12} = W^{23} = 0$. This means that only the angular factors $A^*$, $B^*$ and $C^*$ survive in the electroproduction case.

There is one more simplification that can be made. From electromagnetic current conservation we now that $Q_\mu^* \widetilde{W}^{\mu\nu} = 0$ so $Q_0^* \widetilde{W}^{0\nu} = |\mathbf{Q}^*| \widetilde{W}^{3\nu}$. This means that $\widetilde{W}^{00} = \frac{|\mathbf{Q}^*|^2}{Q_0^{*2}} \widetilde{W}^{33}$ and $\widetilde{W}^{01} = \frac{|\mathbf{Q}^*|}{Q_0^*} \widetilde{W}^{31}$. This gives us the angular factors for electroproduction.

$$A^* = \int \frac{|\mathbf{k}_\pi^*|^2 d|\mathbf{k}_\pi^*|}{E_\pi^*} \left[ \left( \frac{|\mathbf{Q}^*|^2}{Q_0^{*2}} L_{00} + 2 \frac{|\mathbf{Q}^*|}{Q_0^*} L_{03} + L_{33} \right) \widetilde{W}_{(s)}^{33} + \frac{1}{2}(L_{11} + L_{22}) \left( \widetilde{W}_{(s)}^{11} + \widetilde{W}_{(s)}^{22} \right) \right]$$

$$B^* = \int \frac{|\mathbf{k}_\pi^*|^2 d|\mathbf{k}_\pi^*|}{E_\pi^*} 2 \left( L_{01} + \frac{|\mathbf{Q}^*|}{Q_0^*} L_{13} \right) \widetilde{W}_{(s)}^{13}$$

$$C^* = \int \frac{|\mathbf{k}_\pi^*|^2 d|\mathbf{k}_\pi^*|}{E_\pi^*} \frac{1}{2}(L_{11} - L_{22}) \left( \widetilde{W}_{(s)}^{11} - \widetilde{W}_{(s)}^{22} \right)$$

These angular factors can be worked out more precisely. For more detail we refer to the book by Amaldi, Fubini and Furlan [28]. In short by using the identities $Q^2 = -(k - k')^2 \approx 2|\mathbf{k}||\mathbf{k}'|(1 - \cos(\theta_l)) = 4|\mathbf{k}||\mathbf{k}'| \sin^2\left(\frac{\theta_l}{2}\right)$, the expressions for $k^*$ and $k'^*$, and defining the transverse polarization $\epsilon = \frac{1}{1 - \frac{2|\mathbf{Q}|^2}{Q^2} tan^2\left(\frac{\theta_l}{2}\right)}$ , one can find that

$$L_{00} = |\mathbf{Q}^*|^2 \frac{\epsilon}{1 - \epsilon}$$

$$L_{03} = -Q_0^* |\mathbf{Q}^*| \frac{\epsilon}{1 - \epsilon}$$

$$L_{33} = Q_0^{*2} \frac{\epsilon}{1 - \epsilon}$$

$$L_{11} = \frac{Q^2}{2} \frac{1 + \epsilon}{1 - \epsilon}$$

$$L_{22} = \frac{Q^2}{2}$$

$$L_{01} = -\frac{|\mathbf{Q}^*|\sqrt{Q^2}}{2}\frac{\sqrt{2\epsilon(1+\epsilon)}}{1-\epsilon}$$
$$L_{31} = \frac{Q_0^*\sqrt{Q^2}}{2}\frac{\sqrt{2\epsilon(1+\epsilon)}}{1-\epsilon}$$

Bringing it together, and defining the longitudinal polarization $\epsilon_L = -\frac{Q^2}{Q_0^{*2}}\epsilon$, we find

$$L_{\mu\nu}W^{\mu\nu} = \frac{Q^2}{1-\epsilon}\left[\frac{\widetilde{W}_{(s)}^{11}+\widetilde{W}_{(s)}^{22}}{2} + \widetilde{W}_{(s)}^{33}\epsilon_L + \frac{\widetilde{W}_{(s)}^{11}-\widetilde{W}_{(s)}^{22}}{2}\epsilon\cos(2\phi_\pi^*) - \widetilde{W}_{(s)}^{13}\sqrt{2\epsilon_L(1+\epsilon)}\cos(\phi_\pi^*)\right]$$

Similar to the neutrinoproduction case, we can do the integration over $|\mathbf{k}_\pi^*|$ and $p'$. We define an analogous contraction $L_{\mu\nu}\mathcal{H}^{\mu\nu}$, which is obtained from the above expression by the substitution $\widetilde{W} \to \widetilde{\mathcal{H}}$. After doing that the cross section results in:

$$\begin{aligned}\frac{d^5\sigma}{dE_l' d\Omega_l d\Omega_\pi^*} &= \frac{\alpha^2}{32\pi^3}\frac{|\mathbf{k}'|}{|\mathbf{k}|}\frac{1}{Q^4}\frac{\mathbf{k}_\pi}{MW}L_{\mu\nu}\mathcal{H}^{\mu\nu} \\ &= \frac{\alpha}{2\pi^2}\frac{|\mathbf{k}'|}{|\mathbf{k}|}\frac{1}{Q^2}\frac{1}{1-\epsilon}|\mathbf{Q}|\left[\frac{\alpha}{16\pi M|\mathbf{Q}|}\frac{|\mathbf{k}_\pi^*|}{W}\left(\frac{1-\epsilon}{Q^2}\right)L_{\mu\nu}\mathcal{H}^{\mu\nu}\right]\end{aligned}$$

The first factor is sometimes written as $\Gamma_{em}$ and the latter is the photoproduction cross section, as we will see in the next section.

## 2.5 Kinematics of Photoproduction

The case of photoproduction is the limit case where the exchanged virtual photon becomes real ($Q^2 = 0$). So in essence it's the process

$$\gamma(Q) + N(p) \to N'(p') + \pi(k_\pi)$$

where the photon is real instead of virtual and the leptonic part of the reaction is left out.

The derivation for the cross section is very analogous to the earlier cases, but now the lepton tensor is gone and replaced by a product of the photon polarisation vectors. The squared matrix element, summed over final spin and averaged over initial spin becomes:

$$\sum|\mathcal{M}|^2 = \frac{1}{2}\sum_\lambda e^2\mathcal{H}^{\mu\nu}\epsilon_\mu^\lambda\epsilon_\nu^{*\lambda} = \frac{1}{2}e^2(\mathcal{H}^{11}+\mathcal{H}^{22})$$

in which $\mathcal{H}_{\mu\nu}$ is the hadron tensor, and $\lambda$ is the polarisation. The latter equality holds for both linearly and circularly polarised photons.

The cross section is also a tiny bit different, as there is no $k'$ to integrate over. The expression we have instead is:

$$\sigma = \int\frac{(2\pi)^4}{4M|\mathbf{Q}|}|\mathcal{M}|^2\delta^4(Q+p-k_\pi-p')\frac{d^3\mathbf{p}'}{(2\pi)^3 2E_N'}\frac{d^3\mathbf{k}_\pi}{(2\pi)^3 2E_\pi}$$

We can do the usual integrating over $d^3\mathbf{p}'$ to reduce the four-dimensional delta function and then integrating over $|\mathbf{k}_\pi|$ to get rid of the delta function over the energies (and going to the center-of-mass frame). All this, together with the introduction of the fine structure constant $\alpha = \frac{e^2}{4\pi}$ gives us the final differential cross section

$$\frac{d\sigma}{d\Omega} = \frac{\alpha}{16\pi M|\mathbf{Q}|}\frac{|\mathbf{k}_\pi^*|}{W}\frac{1}{2}(\mathcal{H}^{11} + \mathcal{H}^{22})$$

with the photon momentum given by $|\mathbf{Q}| = \frac{W^2-M^2}{2M}$ and $|\mathbf{k}_\pi^*| = \frac{\sqrt{\lambda}}{2W}$ as before.

Notice that this is indeed the same expression as we found inside the electroproduction cross section (where it is multiplied by a factor $\Gamma_{em}$). In this case only the first term in the expansion $L_{\mu\nu}\mathcal{H}^{\mu\nu}$ survives.

As a final note, this differential cross section is often rewritten as a function of Mandelstam variable t. Remember its definition of $t = (Q - k_\pi)^2 = m_\pi^2 - 2E_\gamma^* E_\pi^* + 2|\mathbf{Q}^*||\mathbf{k}_\pi^*|\cos\theta$ and, after integrating over the azimuthal angle $\phi$, we use it to rewrite the cross section as

$$\frac{d\sigma}{dt} = \frac{1}{64\pi s}\frac{1}{|p_i^*|^2}|\mathcal{M}|^2$$

Note that this result holds only for the unpolarised photons, as we summed the matrix element over the polarisations. In the case of a polarised incident photon, there is no summation.

We have every kinematic formula we will need in this work, so now our attention turns towards the missing ingredient: a description of the matrix element $\mathcal{M}$ (and to be more precise the relevant current operators). In the next chapter we will look at a possible high-energy description: Regge theory.

# Chapter 3

# Regge Theory

## 3.1 Motivation behind Regge Theory

Regge theory is an example of a t-channel model, a model that describes hadronic processes in terms of a t-channel exchange of 'something'. In the simplest t-channel models this exchanged something is a particle: a photon in the case of electromagnetic interactions and mesons when describing nuclear forces. Regge theory comes into play at high energies, when this simple picture breaks down. [29]

To see how this 'breaking down' occurs, we will look at a 2 body process $1 + 2 \to 3 + 4$. By looking at the data for such processes there seems to be a connection between a peak at small $|t|$ in s-channel processes and t-channel exchange of particles. So we can try to describe the scattering amplitude using these exchanges. To simplify a bit we consider spinless particles and equal masses $m_1 = m_2 = m_3 = m_4$. The t-channel partial wave expansion of the scattering amplitude is

$$\mathcal{M}(s,t) \sim \sum_{l=0}^{\infty} (2l+1)\mathcal{M}_l(t)P_l(z_t)$$

with

$$z_t = \cos\theta_t = 1 + \frac{2s}{t - 4m^2}$$

and $P_l(x)$ the $l$-th Legendre polynomial. Now suppose that there is only one exchanged particle with a given spin $J$, so the sum reduces to a single term. In the large s limit

$$\mathcal{M}(s,t) \sim (2J+1)\mathcal{M}_J(t)P_J(z_t)$$

A property of Legendre polynomials for large $x$ is

$$P_l(x) \sim x^l$$

which we can use in the scattering amplitude,

$$\mathcal{M}(s,t) \sim f(t) P_J \left(1 + \frac{2s}{t - 4m^2}\right) \sim f(t) s^J$$

The cross section is related to this amplitude by the optical theorem. This theorem, at large s, states that

$$\sigma^{tot}(s) \sim s^{-1} \text{ Im } \mathcal{M}(s, t = 0)$$

Applying this to the particle exchange scattering amplitude, we can make some predictions. For a spin-0 meson, such as the pion, the total cross section would decrease as $s^{-1}$, while the exchange of a spin-1 meson, like the rho meson, gives a total cross section that is constant.

But when we experimentally observe the total cross sections, none of these predictions are confirmed. This illustrates how, in the high-energy limit, the simple picture of particle exchange is not sufficient to predict the cross section.

Regge Theory overcomes the drawback of simple particle exchanges while still using the idea of t-channel exchanges. In Regge Theory the large s-limit of hadronic processes are determined by the exchange of regge trajectories in the t-channel. Regge trajectories are used in a way to combine a whole family of particle resonances acting simultaneously and correlated with each other.

## 3.2 General Regge Theory

In the following paragraphs we will do a basic review of Regge Theory. For a more in-depth exploration of this theory we refer to references [29][30][31].

The idea of Regge theory is to analytically continue the relativistic partial wave amplitudes $\mathcal{M}_l(t)$ to $\mathcal{M}(l,t)$, a function of complex values of $l$. Under the assumption that the potential is well-behaved the function $\mathcal{M}(l,t)$ has singularities in the $l$-plane that are poles, called Regge poles. These obey the simple relation: $l = \alpha(t)$. The function $\alpha(t)$ is called the Regge trajectory and comprises of a family of bound states or resonances, with energies given by $l = \alpha(t)$ for integer $l$. That is the general idea which we will develop mathematically in the rest of this section.

So assume we can continue the partial wave amplitude $\mathcal{M}_l(t)$ to complex $l$-values and construct the interpolating function $\mathcal{M}(l,t)$ which reduces to $\mathcal{M}_l(t)$ for integer $l$. Additionally we suppose that $\mathcal{M}(l,t)$ only has isolated singularities in the complex $l$-plane, that $\mathcal{M}(l,t)$ is holomorphic for $Re(l) \geq L$ ($L$ is some real number) and that $\mathcal{M}(l,t) \to 0$ as $|l| \to \infty$ (for $Re(l) > 0$). It can be shown that such a function does exist and is uniquely determined by the value it takes for integer $l$. We can rewrite the partial wave expansion

$$\mathcal{M}(s,t) = \sum_{l=0}^{\infty} (2l+1) \mathcal{M}_l(t) P_l(z_t)$$

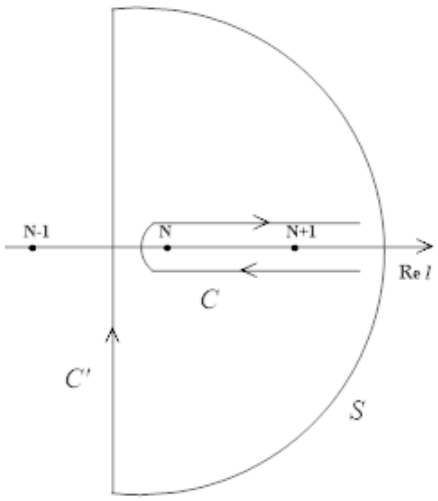


Figure 3.1: Illustration of the contour integral C and its deformation C' + S.

in an equivalent form using the residue theorem

$$\mathcal{M}(s,t) = \sum_{l=0}^{N-1} (2l+1)\mathcal{M}_l(t)P_l(z_t) - \frac{1}{2i}\int_C (2l+1)\mathcal{M}(l,t)\frac{P_l(-z_t)}{\sin(\pi l)}dl$$

where the residues of $\sin(\pi l)$ are $\frac{(-1)^l}{\pi}$ (for integer l) and $P_l(-z) = (-1)^l P_l(z)$. The contour C wraps around the real axis, avoiding all singularities of $\mathcal{M}(l,t)$.

The contour can be deformed into a contour C' + S, where C' is $(L-i\infty, L+i\infty)$ and S is the semicircle at infinity. This contour still avoids all singularities of $\mathcal{M}(l,t)$. Because of the asymptotic behavior of Legendre polynomials at large $l$ and our assumption $\mathcal{M}(l,t) \to 0$ as $|l| \to \infty$, the integral over S vanishes and only the integral over C' survives:

$$\mathcal{M}(s,t) = \sum_{l=0}^{N-1} (2l+1)\mathcal{M}_l(t)P_l(z_t) - \frac{1}{2i}\int_{L-i\infty}^{L+i\infty} (2l+1)\mathcal{M}(l,t)\frac{P_l(-z_t)}{\sin(\pi l)}dl$$

Now we displace the contour C' to the left. As we include extra poles in our contour, their residues need to be subtracted from the integral. For the remaining residues of $\frac{1}{sin(\pi l)}$ this merely cancels out the summation, but we are left with the residues of the singularities of $\mathcal{M}(l,t)$. We push down the contour to C' $= (c - i\infty, c + i\infty)$ with $-\frac{1}{2} \leq Re(c) < 0$,

$$\mathcal{M}(s,t) = -\sum_i \pi(2\alpha_i(t)+1)\beta_i(t)\frac{P_{\alpha_i}(-z_t)}{\sin(\pi\alpha_i)} - \frac{1}{2i}\int_{c-i\infty}^{c+i\infty} (2l+1)\mathcal{M}(l,t)\frac{P_l(-z_t)}{\sin(\pi l)}dl$$

This is the Watson-Somerfeld representation of the scattering amplitude. $\alpha_i(t)$ is the location of the i-th pole of $\mathcal{M}(l,t)$ in the complex $l$-plane, a Regge pole, while $\beta_i(t)$ is the residue at that pole.

For fixed t and large s the remaining integral scales as $|z_t|^{-\frac{1}{2}}$, which can be neglected so that only the pole series survives. This assumption is crucial for the rest of the Regge framework to function, so we will have to keep in mind that Regge theory is only valid for large enough s.

After using some properties of the Legendre polynomials, we end up with

$$\begin{aligned}\mathcal{M}(s,t) &\sim -\pi \sum_i \beta_i(t) \frac{1}{\Gamma(\alpha_i(t)+1)\sin(\pi\alpha_i(t))} s^{\alpha_i(t)} \\ &= \sum_i \beta_i(t)\Gamma(-\alpha_i(t)) s^{\alpha_i(t)}\end{aligned}$$

where we used the property $\Gamma(\alpha_i(t)+1)\Gamma(-\alpha_i(t)) = -\pi/\sin(\pi\alpha_i(t))$.

We need two more corrections. First it is considered bad practice to raise a quantity like s to a power, so we make it into the dimensionless quantity $s^*$. This can be done by introducing a fixed scale $s_0$ or by using the parameter $\alpha'$ as a scale. We will explore both options in this thesis. Furthermore, in relativistic scattering, an extra quantum number $\xi$ $(= \pm 1)$ is introduced, and a phase factor is added to the Regge pole contributions. So we end up with

$$\mathcal{M}(s,t) \sim \sum_i \beta_i(t)\Gamma(-\alpha_i(t)) \frac{1+\xi e^{-i\pi\alpha_i(t)}}{2} \left(s^*\right)^{\alpha_i(t)}$$

The expression above holds for spinless exchanged particles but needs to be slightly amended for spin 1 particles (vector mesons):

$$\mathcal{M}(s,t) \sim \sum_i \beta_i(t)\Gamma(1-\alpha_i(t)) \frac{1+\xi e^{-i\pi\alpha_i(t)}}{2} \left(\frac{s}{s_0}\right)^{\alpha_i(t)-1}$$

Regge trajectories can only be determined experimentally and are usually written in the form $\alpha(t) = \alpha_0 + \alpha' t$ or sometimes $\alpha(t) = \alpha'(t - m_x^2)$ for trajectory of particle species x. The different Regge trajectories we use in this work are described in Chapter 4.

## 3.3 Reggeized Born term model

At this point we have found a high energy expression for the relativistic matrix element by using Regge theory, but it is important to inspect more closely what we have gained. We know the high energy $s$-behavior, from experimental efforts we got the Regge trajectories, but the unknown factor is the residue $\beta_i(t)$, the $t$-behavior of the scattering amplitude. That residue is not provided by Regge theory, so it is in describing this residue that different models can be introduced.

One possible path to take is splitting the residue in different invariant amplitudes, with a certain $t$-dependence [32]. These amplitudes are then linked to

certain kinds of Regge trajectories. The amplitudes in this approach contain a lot of parameters and these need to be fit to the available data. This approach works as [32] demonstrates, with fits to the data that are very good, better than our model. But using their approach, there is a disadvantage for our purposes in this work. The plethora of parameters requires a good amount of data to fit the model. In our case the goal is a description of neutrino-induced pion production, which has very limited data, and in particular neutral current SPP, a process that up to this point has not been measured experimentally. We simply don't have enough data to be able to fit a lot of parameters, so we look for another way to model the residues.

Consider what happens to the Regge scattering amplitude when $t \approx m_x^2$. In that case the amplitude reduces to something that scales as $\frac{s^J}{t-m_x^2}$, where $J$ is the spin of particle x. We recover the meson-exchange born term! So we presume that the rest of the Regge scattering amplitude must also reduce to the Born terms in that limit. Inspired by that observation, a recipe was proposed to go from a low energy interaction model to a Regge model: replace the Feynman propagator $\frac{1}{t-m^2}$ in the low energy model by a Regge propagator $\Gamma(1-\alpha_i(t))(1+\xi e^{-i\pi\alpha_i(t)})\,(s^*)^{\alpha_i(t)}$. [35]

Chiral Perturbation Theory is a possible candidate for such a low energy model, as is done in [20]. There they take the background terms for pion production in ChPT and reggeize them by the recipe above. This approach works quite well, but only in the case of charged pion production, as there are no background terms that can be used to explain the production of neutral pions. Still this work is interesting to us, as it points out that we need both a pion and a rho trajectory to explain the observed cross sections.

In this work we let go of ChPT and explicitly introduce the tree-level Feynman diagrams that are possible for pion production at the nucleon vertex (Born terms). In essence we expand the frame of [20] by explicitly including more particle exchanges (when they are allowed). Of course we cannot just do that and expect the model to be functional, which is why we first check this model, which is also known as the Reggeized Born term model, with the available photoproduction and electroproduction data.

The big advantage of relying on the Born terms is that we can use a model were the parameters are the different coupling constants and thus already constrained by various other experiments. Using Regge propagators instead of Feynman propagators now allows us to take into account the contributions of the more massive, high-spin particle exchanges. In the following chapters we will begin to apply our model.

# Chapter 4

# Photoproduction

A first test of the Reggeized Born term model we use is pion photoproduction, which is the $Q^2 = 0$ limit of pion electroproduction. Our model is based primarily on the work of Guidal, Laget and Vanderhaegen[21]. They constructed the first Reggeized Born term model that could describe photoproduction data reasonably well. In this chapter we will reproduce their results and compare it to the available data, building up the relevant Regge trajectories and currents. We will also make use of later work done by Kaskulov and Mosel [22][23]. They extended the model to electroproduction, but had some slightly different diagrams. Finally there is a third reference by Kamano, Nakamura, Lee and Sato[33], that describes the different currents in more detail, building them up from the relevant vertex interactions. We will use that work as a third source of coupling constants. We explore these differences (in constants and diagrams) and compare between them.

## 4.1 Charged pion photoproduction

There are two reactions featured in this section:

$$\gamma + p \to \pi^+ + n$$

and

$$\gamma + n \to \pi^- + p$$

Both reactions are described by the same exchange diagrams, only differing in small details like isospin signs and Regge phases. As a rule of thumb, all figures shown in this section are calculated on $\pi^+$ appearance reactions, unless explicitly stated otherwise.

### 4.1.1 Pion exchange

The most important contribution to the charged pion photoproduction is the Pion exchange diagram. The hadron current for this process (which is inserted

in the hadron tensor) is:

$$\mathcal{O}^{\mu}_{\pi,t} = \mathcal{I}\ g_{\pi NN}\left((q^{\mu}-k^{\mu}_{\pi})\gamma^{5}\right)(-\alpha'_{\pi})R^{\pi}_{phase}\Gamma(-\alpha_{\pi}(t))\,(s^{*})^{\alpha_{\pi}(t)}$$

Let's go through this expression piece by piece. $\mathcal{I}$ is the isospin factor, which we'll define later. Next there is the coupling constant of this diagram $g_{\pi NN}$, which is sometimes written as $f_{\pi NN}\frac{2M}{m_{\pi}}$ with $m_{\pi} = 138$ MeV. The slightly different coupling constants used in the works we referenced are summarized in the table below:

| | GLV[21] | KM[24][1] | KNLS[33] |
|---|---|---|---|
| $g_{\pi NN}$ | 13.64 | 13.0 | 13.59 |

The coupling $(q^{\mu}-k^{\mu}_{\pi})\gamma^{5}$ we use is the pseudoscalar (PS) coupling. Equivalently we could have used the pseudovector (PV) coupling $(q^{\mu}-k^{\mu}_{\pi})\gamma^{5}\frac{\not{q}}{2M}$ but then we would also need to include a contact term [34]. We avoid the trouble of doing that by choosing the pseudoscalar coupling.

The last part of the expression is the Regge propagator, where we used $s^{*}$ to mean the dimensionless, rescaled version of $s$. This can be done by either dividing by 1 GeV$^2$ or multiplying by $\alpha'$. The Regge trajectory is given by $\alpha_{\pi}(t) = \alpha'_{\pi}(t-m^2_{\pi})$ and the slope used in the two reference works differs slightly:

| | GLV[21] | KM[22] |
|---|---|---|
| $\alpha'_{\pi}(\text{GeV}^{-2})$ | 0.7 | 0.74 |

By approaching this problem from a Born term perspective we run into problems if we include the t-channel pion diagram all by itself. In the Born term model we have to include more diagrams in order to end up with a gauge invariant amplitude. In our case, when using the PS coupling, we also need to include the s- and u-channel nucleon diagrams (where a nucleon is propagating instead of a pion). As the Reggeized Born term model reduces to the Born term model at $t \approx m^2_{\pi}$, we will have to include these diagrams in our Reggeized model as well. This gauge invariance problem is only present for the pion diagrams as the other $(\rho, \omega, b_1,\ ...)$ t-channel exchange diagrams are gauge invariant by themselves.

However it is not natural to introduce s- and u-channel diagrams in a Regge model that deals with t-channel exchanges. To force it in our model we have to consider what really happens when we Reggeize a diagram. The Feynman propagator is replaced by the Regge propagator, or in other words we multiply the Feynman diagram by $\mathcal{P}_{Regge}(t-m^2_{\pi})$. We can apply this same action to the s- and u-channel diagrams to 'reggeize' them that way.

In the end we are left with the s-channel current:

$$\mathcal{O}^{\mu}_{\pi,s} = \mathcal{I}\ g_{\pi NN}\left(\gamma^{5}\frac{\not{p}_{s}+m_{N}}{s-m^2_{N}}\gamma^{\mu}\right)(t-m^2_{\pi})(-\alpha'_{\pi})R^{\pi}_{phase}\Gamma(-\alpha_{\pi}(t))\,(s^{*})^{\alpha_{\pi}(t)}$$

[1] Technically this value is not from a reference by Kaskulov Mösel, but ref [24] is a refinement of their model, which is why we use that value here. Also it is the only value they change compared to [22].

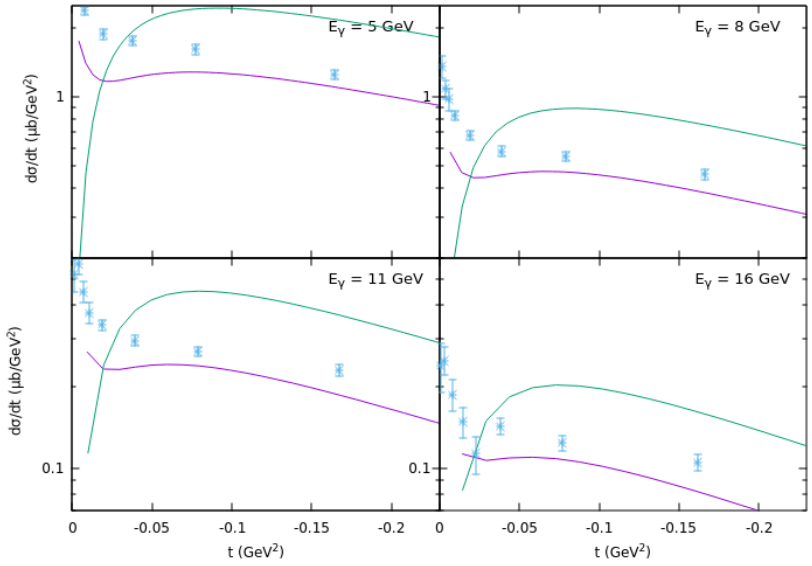


Figure 4.1: Comparison between pion t-channel (green) and pion t + s/u channel (purple) for very small -t. Note that the forward peak is not described by the t-channel diagram alone. Data is from [36]

and similarly the u-channel current:

$$\mathcal{O}^{\mu}_{\pi,u} = \mathcal{I}\; g_{\pi NN} \left( \gamma^{\mu} \frac{\not{p}_u + m_N}{u - m_N^2} \gamma^5 \right) (t - m_\pi^2)(-\alpha'_\pi) R^{\pi}_{phase} \Gamma(-\alpha_\pi(t)) \, (s^*)^{\alpha_\pi(t)}$$

The effect of adding this s- (or u-) channel terms is shown in figure 4.1 for very small $|t|$. It shows that the added terms are needed to explain the peak of the differential cross section at these forward angles.

Before we move on, we take a look at the isospin $\mathcal{I}$. We have used the method described in [33] to calculate the isospin factors $\mathcal{I}$. Our results are summarised in the table below. The convention we use here differs by a factor $-\sqrt{2}i$ compared to [20] as they stated that factor separately in the current. It also differs from [21] and [22] by a global minus sign for the $\pi^-$ reaction, which has no impact on the cross section as only the relative signs between diagrams matter.

For some exchanges we have isospin zero. In theory this is not the true value of the isospin, but for simplicity's sake we put the isospin value at zero to show that this exchange does not contribute. The reason for this is that we are considering the nucleons on their own (and not its constituent quarks) and as is usual we approximate that photons do not couple to neutrons (electric model). Therefore the u-channel diagram cannot contribute to the $\pi^+$ reaction and the

s-channel does not contribute for the $\pi^-$ reaction.

| | t-channel | s-channel | u-channel |
|---|---|---|---|
| $\gamma + p \to \pi^+ + n$ | $-\sqrt{2}i$ | $\sqrt{2}i$ | 0 |
| $\gamma + n \to \pi^- + p$ | $-\sqrt{2}i$ | 0 | $-\sqrt{2}i$ |

### 4.1.2 Rho exchange

Another diagram that is relevant for charged pion production is the rho t-channel exchange, with its current

$$\mathcal{O}^{\mu}_{\rho} = -\mathcal{I} g_{\rho NN} g_{\rho\pi\gamma} \epsilon^{\mu\nu\rho\alpha} Q_{\nu} q_{\rho} (-g_{\alpha\beta}) \left[\gamma^{\beta} - \frac{\kappa_{\rho}}{4m_N}(\gamma^{\beta}\not{q} - \not{q}\gamma^{\beta})\right] \\ (-\alpha'_{\rho}) R^{\rho}_{phase} \Gamma(1 - \alpha_{\rho}(t)) \, (s^*)^{\alpha_{\rho}(t)-1}$$

The factor $\mathcal{I}$ is the isospin factor, for $\gamma + p \to \pi^+ + n$ this is $\mathcal{I} = -\sqrt{\in}$, while in the case of $\gamma + n \to \pi^- + p$ it is $\mathcal{I} = \sqrt{\in}$. The coupling constants $g_{\rho NN}$ and $\kappa_{\rho}$ represent the coupling strength of the strong interaction vertex $\rho NN$ while $g_{\rho\pi\gamma}$ is the coupling at the electromagnetic vertex $\rho\pi\gamma$. The latter is sometimes parametrized as $\frac{g_{\rho\pi\gamma}}{m_{\pi}}$. The different coupling constants used in the works we referenced are summarized in the table below:

| | GLV[21] | KM[22] | KNLS[33] |
|---|---|---|---|
| $g_{\rho NN}$ | 3.4 | 3.4 | 4.724 |
| $\kappa_{\rho}$ | 6.1 | 6.1 | 1.177 |
| $g_{\rho\pi\gamma}(\text{GeV}^{-1})$ | 0.746 | 0.728 | 0.924 |

The rho Regge trajectory is given by $\alpha_{\rho}(t) = \alpha'_{\rho} t - \alpha_{\rho,0}$ and the relevant parameters have values:

| | GLV[21] | KM[22] |
|---|---|---|
| $\alpha'_{\rho}(\text{GeV}^{-2})$ | 0.8 | 0.85 |
| $\alpha_{\rho,0}$ | 0.55 | 0.53 |

The following figures show the effect of adding the rho diagram. In figure 4.2 the $\rho$ contribution is shown, as the only diagram and also combined with the pion diagrams. It is clear that for higher $|t|$ the $\rho$ t-channel exchange is the dominant diagram, which is to be expected given it has a higher trajectory slope.

To get a clearer insight in the way that interference between the diagrams matters, figure 4.3 shows both the combined cross section (with interference) and the sum of the pion and rho diagram cross sections (without interference). Again the effect is most apparent at the higher $|t|$ values, where the interference causes the cross section to lower.

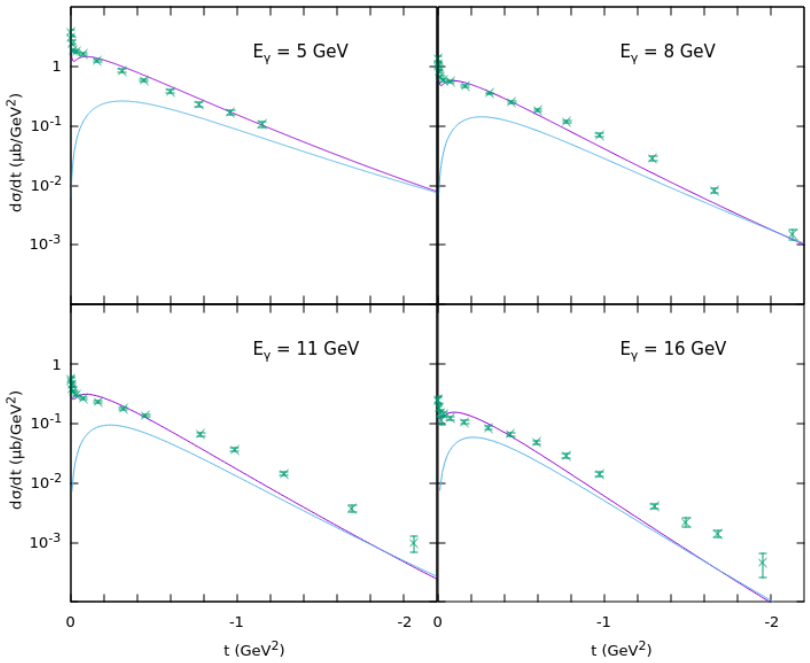


Figure 4.2: The rho diagram contribution is shown on its own (blue) and combined with the pion diagrams. The dominant trajectory goes from pion to rho as $|t|$ increases. Data is from [36].

### 4.1.3 $a_1$ exchange

Only one of our two reference papers ([22]) includes a third trajectory, the $a_1$ trajectory. Its current is

$$\mathcal{O}^{\mu}_{a_1} = \mathcal{I} G_{a_1\pi\gamma} G_{a_1 NN} (Q^{\alpha} q^{\beta} \gamma^{\mu} - q^{\mu} Q^{\alpha} \gamma^{\beta})(-g_{\alpha\beta})\gamma^5(-\alpha'_{a_1})\Gamma(1-\alpha_{a_1}(t)) R^{a_1}_{phase} \, (s^*)^{\alpha_{a_1}(t)-1}$$

with isospin factor $\sqrt{2}i$ for both reactions, $G_{a_1\pi\gamma} = 1.1$ GeV$^{-1}$ and the $a_1$ trajectory is $\alpha_{a_1}(t) = \alpha_{\rho}(t) = (0.85 \text{ GeV}^{-2})t - 0.47$. We have found two values for $G_{a_1 NN}$ given in the following table

| | KM[22] | KNLS[33] |
|---|---|---|
| $G_{a_1 NN}$ | 7.1 | 8.247 |

Though the $a_1$ trajectory can be included in our model it has no perceivable effect on the predicted cross section. Figure 4.4 shows the differential cross section for a model that includes $a_1$ and a model without it. As both curves

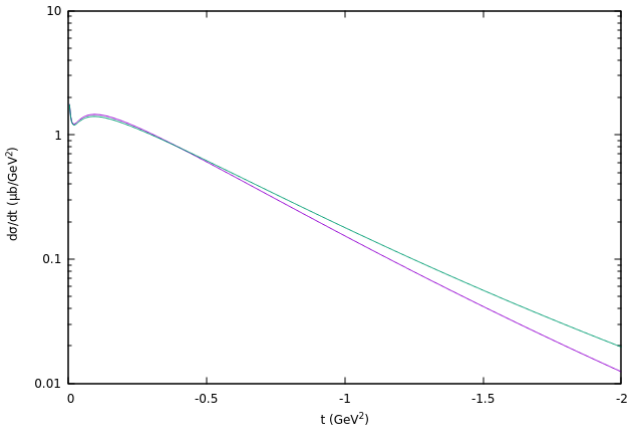


Figure 4.3: Comparison between the combined diagrams with interference (purple) and without interference (green). The effect is most noticeable at high $|t|$. Data is from [36] at photon energy $E_\gamma = 5$ GeV

overlap, without a visible difference between them, we can conclude that the $a_1$ trajectory is not needed to model the cross section.

There is nothing inherently wrong about including this trajectory though, even if it has no observed effect. We choose to include it for completeness' sake.

### 4.1.4 Discussion

We have constructed the different diagrams that combine in charged pion photoproduction and we have seen that there are a number of possible parameter sets to choose from. We will now compare between them.

First of all there are three sets of coupling constants found in the different reference papers. We summarise them here.

| | GLV[21] | KM[22] | KNLS[33] |
|---|---|---|---|
| $g_{\pi NN}$ | 13.64 | 13.0 | 13.59 |
| $g_{\rho NN}$ | 3.4 | 3.4 | 4.724 |
| $\kappa_\rho$ | 6.1 | 6.1 | 1.177 |
| $g_{\rho\pi\gamma}(\text{GeV}^{-1})$ | 0.746 | 0.728 | 0.924 |
| $G_{a_1 NN}$ | / | 7.1 | 8.247 |

Already it is clear that the parameters from GLV[21] and KM[22] only have slight differences, while the parameter set from KNLS[33] is more profoundly different. A comparison between these three is found in figure 4.5. Though there are slight differences between them, they mostly give very similar cross sections. In the next sections we will not discuss the effect of different coupling constants on the cross sections, as the impact is minor, but we will include their different values for completion's sake.

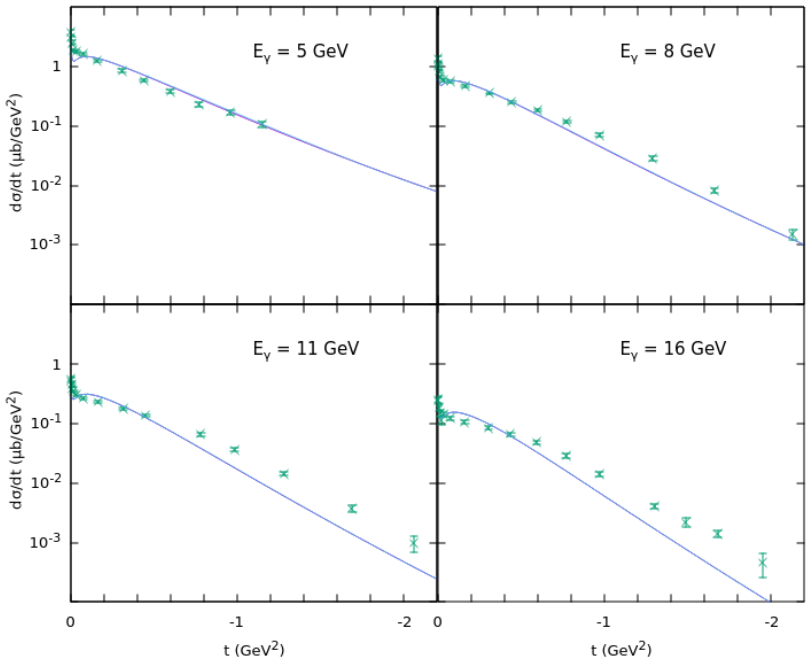


Figure 4.4: Illustration of the very small $a_1$ contribution to the cross section. The purple and green graphs (with and without $a_1$) coincide to a blue graph. Data is from [36]

Besides the coupling constants, there is the more relevant Regge part of our model. First there is the issue of scaling $s$ in order to make it dimensionless. GLV[21] chose to use a static scale $s^* = s/1\ \text{GeV}^2$ while later work [22][20] opted for a dynamic scale using the relevant Regge trajectory slopes $s^* = s\alpha'$. Besides the scale choice, there are also slight differences in the Regge trajectory parameters, which we summarize in the table below

| | GLV[21] | KM[22] |
|---|---|---|
| $\alpha'_\pi(\text{GeV}^{-2})$ | 0.7 | 0.74 |
| $\alpha'_\rho(\text{GeV}^{-2})$ | 0.8 | 0.85 |
| $\alpha_{\rho,0}$ | 0.55 | 0.53 |

In figure 4.6 we compare these different choices. The purple and orange curves use the dynamic scale while the yellow and blue curves represent static scale. For the GLV parameters there are the blue and orange curves and for the KM parameters the purple and yellow ones.

There are no easy conclusions to be made from this comparison. For larger $|t|$ and high $E_\gamma$ the dynamic scales seem to be favoured, but over all energies, the

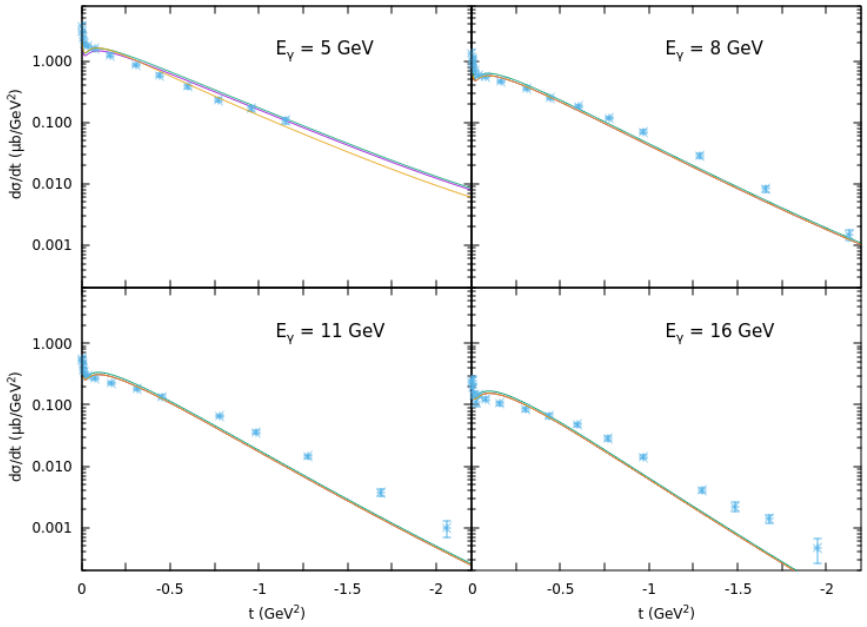


Figure 4.5: Illustration of the different coupling constants. The green curve is GLV values, the purple curve is KM constants and the orange graph uses KNLS. There is no significant difference between them. Data is from [36].

more forward region (smaller $|t|$) is better described by the static scale (combined with KM parameters). We will keep these observations in mind when we do a similar comparison for neutral pion photoproduction.

Finally we have to discuss Regge phase. An isolated trajectory has a phase $\frac{1+\xi e^{-i\pi\alpha_i(t)}}{2}$. But often in Regge theory there are two trajectories that are degenerate, meaning that they have nearly exactly the same shape of trajectory. The only difference is in their phase, as they have opposite signatures.

To simplify, these trajectories can be added up together, either with a relative plus or minus sign between them and doing so we end up with a rotating $R^i_{phase} = e^{-i\pi\alpha_i(t)}$ or a constant phase $R^i_{phase} = 1$. For the charged pion production, both the $b_1(1235)$ and the $a_2(1320)$ trajectories, the corresponding trajectories for $\pi$ and $\rho$, are allowed, so both of them will be degenerate. For $a_1$, ref.[22] argues that there is not enough evidence to allow us to take into account $\rho_2$, so $a_1$ will stay non-degenerate. In our case we follow the convention from [22], and use phases:

| | $\gamma + p \to \pi^+ + n$ | $\gamma + n \to \pi^- + p$ |
|---|---|---|
| $\pi + b_1$ | $e^{-i\pi\alpha_\pi(t)}$ | 1 |
| $\rho + a_2$ | $-e^{-i\pi\alpha_\rho(t)}$ | 1 |
| $a_1$ | $\frac{1-e^{-i\pi\alpha_{a_1}(t)}}{2}$ | $\frac{1-e^{-i\pi\alpha_{a_1}(t)}}{2}$ |

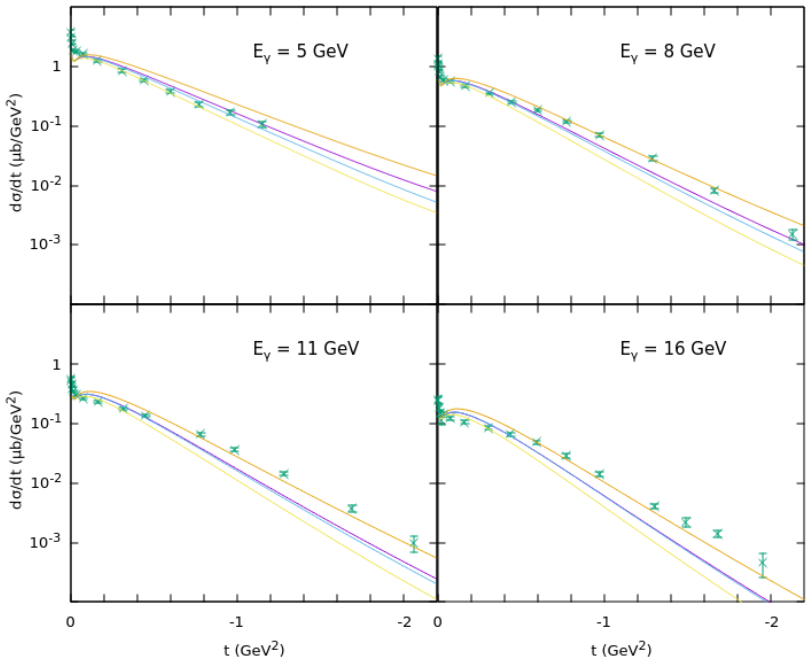


Figure 4.6: Illustration of the different Regge choices. From above to below: GLV + dynamic scale (orange), KM + dynamic scale (purple), GLV + static scale (blue) and KM + static scale (yellow). Data is from [36]

## 4.2 Neutral pion photoproduction

There are two reactions described in this section:

$$\gamma + p \to \pi^0 + p$$

and

$$\gamma + n \to \pi^0 + n$$

Just like for charged pion photoproduction, these reactions are described by the same diagrams, only differing in small details, which will be clearly stated. When figures show up, they were calculated from the proton-reaction. That is because the neutron initial state reactions are hard to observe experimentally, as there are no free neutron targets. For neutral pion production there is even no experimental data for the $\pi^0 n$ final state[37], so we have nothing to compare our model to.

### 4.2.1 Omega exchange

The dominant diagram in neutral pion photoproduction is the omega exchange diagram, which has a current

$$\mathcal{O}^{\mu}_{\omega} = -\mathcal{I} g_{\omega NN} g_{\omega\pi\gamma} \epsilon^{\mu\nu\rho\alpha} Q_{\nu} q_{\rho} (-g_{\alpha\beta}) \gamma^{\beta} (-\alpha'_{\omega}) R^{\omega}_{phase} \Gamma(1-\alpha_{\omega}(t)) \, (s^{*})^{\alpha_{\omega}(t)-1}$$

with isospin $\mathcal{I} = 1$ and again the 2 coupling constants $g_{\omega NN}$ and $g_{\omega\pi\gamma}$ coming from the vertices $\omega NN$ and $\omega\pi\gamma$. The current has exactly the same structure as the rho current, but with $\kappa_{\omega} = 0$, which is obvious as both are vector mesons of the same spin, so with similar behavior. Note that in [33] $\kappa_{\omega} \neq 0$, so then the expression has to include the whole current like in the $\rho$ exchange.

The different coupling constants in the various reference works are given as

| | GLV[21] | KM[23][2] | KNLS[33] |
|---|---|---|---|
| $g_{\omega NN}$ | 15 | 18 | 5.48 |
| $\kappa_{\omega}$ | 0 | 0 | 0.944 |
| $g_{\omega\pi\gamma}(\text{GeV}^{-1})$ | 2.28 | 2.4 | 1.52 |

The omega Regge trajectory is given by $\alpha_{\omega}(t) = \alpha'_{\omega} t - \alpha_{\omega,0}$ and the relevant parameters have values:

| | GLV[21] | KM[23] |
|---|---|---|
| $\alpha'_{\omega}(\text{GeV}^{-2})$ | 0.9 | 0.85 |
| $\alpha_{\omega,0}$ | 0.44 | 0.4 |

### 4.2.2 Rho exchange

The second important diagram for neutral pion photoproduction is the rho exchange. The current is of the exact same structure as in the charged pion case.

$$\begin{aligned}\mathcal{O}^{\mu}_{\rho} = &- \mathcal{I} g_{\rho NN} g_{\rho\pi\gamma} \epsilon^{\mu\nu\rho\alpha} Q_{\nu} q_{\rho} (-g_{\alpha\beta}) \left[\gamma^{\beta} - \frac{\kappa_{\rho}}{4m_N} (\gamma^{\beta} \not{q} - \not{q} \gamma^{\beta})\right] \\ &(-\alpha'_{\rho}) R^{\rho}_{phase} \Gamma(1-\alpha_{\rho}(t)) \, (s^{*})^{\alpha_{\rho}(t)-1}\end{aligned}$$

There are a number of small differences in the details. First the isospin is of a different value (which is nothing illogical as it concerns different nucleon combinations), with $\mathcal{I} = 1$ for $\gamma + p \to \pi^0 + p$, while $\mathcal{I} = -1$ for the reaction $\gamma + n \to \pi^0 + n$. Then there is the matter of the coupling constants. The values for $g_{\rho NN}$ are exactly the same as in charged pion photoproduction (so we will not repeat them here), but $g_{\rho\pi\gamma}$ is more curious. While [33] offers no alternative value for the neutral pion case, [23] does give us a different value: $g_{\rho\pi\gamma} = 0.84$ GeV$^{-1}$, which is bigger than their charged pion value. In [21] it is less obvious. They do not explicitly state another value but in their discussion

[2]The neutral pion case was worked out by Kaskulov in [23], but for simplicity's sake we will keep calling it the KM model, as it was inspired by their previous work on the charged pion

about the $b_1$ coupling constants they give the relation $g_{b_1^0\pi\gamma} = \sqrt{2}g_{b_1^\pm\pi\gamma}$ and say that relation is well verified for the rho meson. Assuming they also used it for the rho meson, we come up with a third possible value: $g_{\rho\pi\gamma} = 1.06\ \text{GeV}^{-1}$.

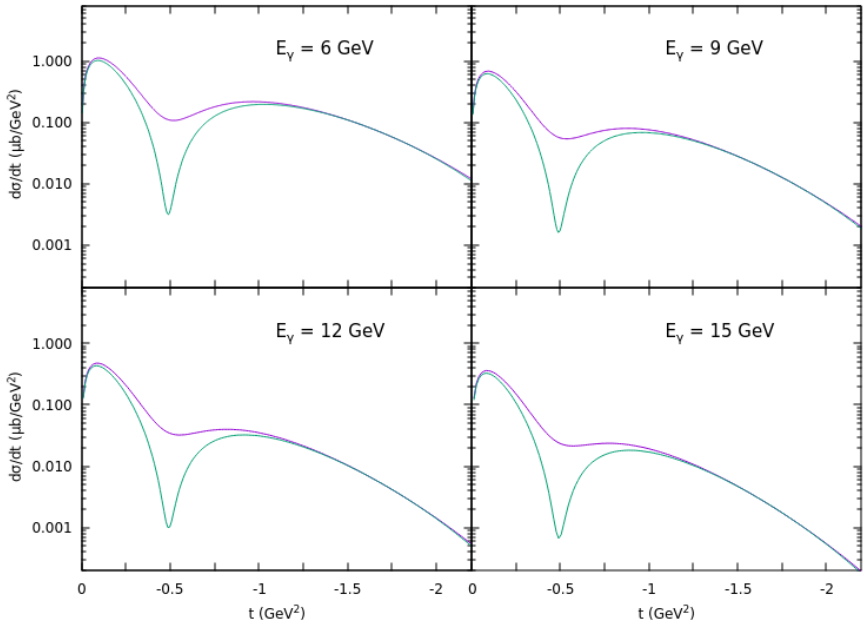


Figure 4.7: Illustration of Regge phase. Purple graph is the degenerate $\rho$ trajectory and the green curve is non-degenerate, with very obvious dips.

Before we can move on to other diagrams we have to address the Regge phases of the two dominant diagrams. Our two sources agree on a non-degenerate phase for omega ($\frac{1-e^{-i\pi\alpha_\omega(t)}}{2}$), but on the rho phase they disagree. While [21] goes with a similar degeneracy scheme as in the charged pion case, which is a rotating phase for incident protons, [23] uses a non-degenerate phase. This small change in phase has a big effect on the cross section as non-degenerate phases cause dips to appear in the cross section, where the phase goes to zero. As an illustration, figure 4.7 shows the sum of the rho and omega diagrams with a degenerate and non-degenerate rho trajectory.

### 4.2.3 Nucleon channels

Another big difference between the two reference works is that [23] includes the s/u-channel Born terms in his model. The current, given below, is exactly the same as in the charged pion case, with the obvious exception of isospin factors: $\mathcal{I} = -i$ for the outgoing proton reaction and $\mathcal{I} = i$ for the outgoing neutron

reaction. All the other values, including the Regge phases, are unchanged.

$$\mathcal{O}_s^\mu = \mathcal{I}\ g_{\pi NN}(t-m_\pi^2)\left(\gamma^5\frac{(\not{p}_s+m_N)}{s-m_N^2}\gamma^\mu\right)(-\alpha'_\pi)R^\pi_{phase}\Gamma(-\alpha_\pi(t))\,(s^*)^{\alpha_\pi(t)}$$

$$\mathcal{O}_u^\mu = \mathcal{I}\ g_{\pi NN}(t-m_\pi^2)\left(\gamma^\mu\frac{\not{p}_u+m_N}{u-m_N^2}\gamma^5\right)(-\alpha'_\pi)R^\pi_{phase}\Gamma(-\alpha_\pi(t))\,(s^*)^{\alpha_\pi(t)}$$

The primary advantage to include this diagram is that it fills up the dips (caused by non-degenerate rho) in the cross sections. In the following figure 4.8, we compare these two approaches: degenerate rho on the one hand, non-degenerate rho and s/u-channel on the other hand.

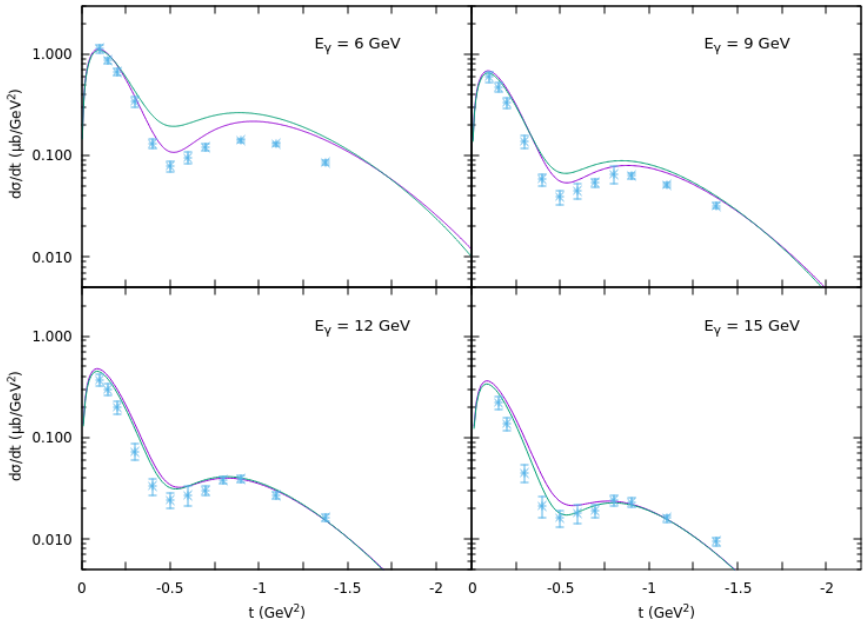


Figure 4.8: Comparison of cross section between the models of [23] and [21]. Green is the KM model with non-degenerate rho and nucleon channel diagrams and purple is the model from GLV with degenerate rho. Data is from [38]

As a first conclusion from these cross sections, it looks like the GLV model works better at the lower $W$, while the KM model is slightly superior at the higher $W$. The big difference is, as expected, to be found in the dip region around $t \approx -0.5$ GeV$^2$. As of now, we cannot conclusively choose one model to be superior over the other, so we will return to the comparison later.

A possible disadvantage of relying on nucleon channels to fill in the dips is the neutron reaction. In our hadronic physics framework photons do not couple to neutrons, so there is no possibility of a non-zero s- or u-channel contribution when the initial nucleon is a neutron. Of course, lacking any data, we cannot

conclusively state that the KM model would not describe the data, but there are reasons to be wary.

### 4.2.4 $b_1$ exchange

A final t-channel exchange diagram that is included is that of the b1 current, given by [21] as

$$\mathcal{O}^{\mu}_{b_1} = \mathcal{I} g_{b_1\pi\gamma} \frac{g_{b_1 NN}}{m_\pi} (Q^\alpha q^\beta \gamma^\mu - q^\mu Q^\alpha \gamma^\beta)(-g_{\alpha\beta})\gamma^5(-\alpha'_{b_1}) R^{b_1}_{phase} \Gamma(1-\alpha_{b_1}(t))\,(s^*)^{\alpha_{b_1}(t)-1}$$

with coupling constants $g_{b_1\pi\gamma} = 0.122$ and $g_{b_1 NN} = 16.44$.

A very similar expression is found in [22]

$$\mathcal{O}^{\mu}_{b_1} = i\mathcal{I} G_B (Q^\alpha q^\beta (p^\mu + p'^\mu) - q^\mu Q^\alpha (p^\beta + p'^\beta))(-g_{\alpha\beta})\gamma^5(-\alpha'_{b_1}) R^{b_1}_{phase} \Gamma(1-\alpha_{b_1}(t))\,(s^*)^{\alpha_{b_1}(t)-1}$$

with one coupling constant (that absorbed the effect of both vertices) $G_B = 11\ \text{GeV}^{-2}$. The isospin is $\mathcal{I} = 1$ for $\gamma + p \to \pi^+ + n$, while $\mathcal{I} = -1$ for $\gamma + n \to \pi^- + p$.

The $b_1$ trajectory is presumed to be the same as the $\pi$ trajectory seen before: $\alpha_{b_1}(t) = \alpha'_\pi(t - m^2_\pi)$.

Similar to the $a_1$ trajectory in charged pion production processes, the $b_1$ exchange has quite a limited effect on the cross section as a whole. This is illustrated in the following figure (which uses the GLV diagrams). A similar tiny contribution is seen when using KM currents.

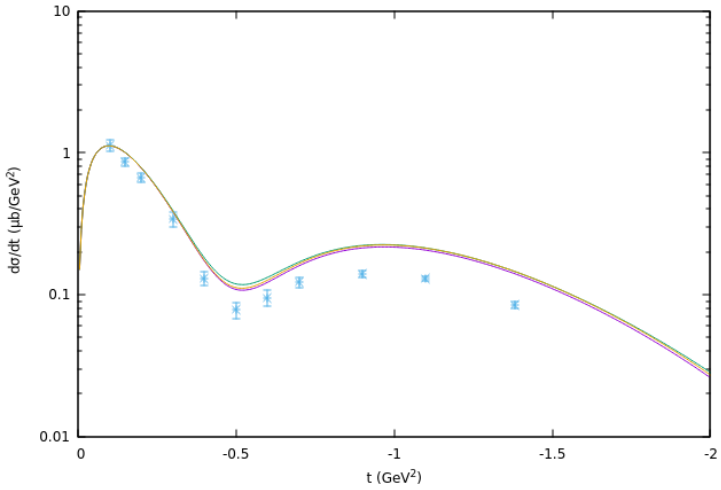


Figure 4.9: Illustration of the small effect of the $b_1$ exchange for $E_\gamma = 6$ GeV. Purple is the cross section without it, green uses degenerate $b_1$, wile orange has non-degenerate $b_1$. Data is from [38]

In the figure we have included 2 possible phases, a degenerate and a non-degenerate. It is quite clear that no matter which choice we make, the contribution stays very small. As the corresponding $\pi$ trajectory is not allowed for neutral pion production, it seems that $b_1$ cannot be degenerate, so in the rest of this work we use the non-degenerate phase

$$R^{b_1}_{phase} = \frac{1 - e^{-i\pi\alpha_{b_1}(t)}}{2}$$

### 4.2.5 Discussion

Just like for charged pion production, there are a number of parameters to look out, more specifically the Regge parameters. To make a comprehensive comparison between them we will look at their effect for both the GLV currents, in figure 4.10 and KM currents, in figure 4.11.

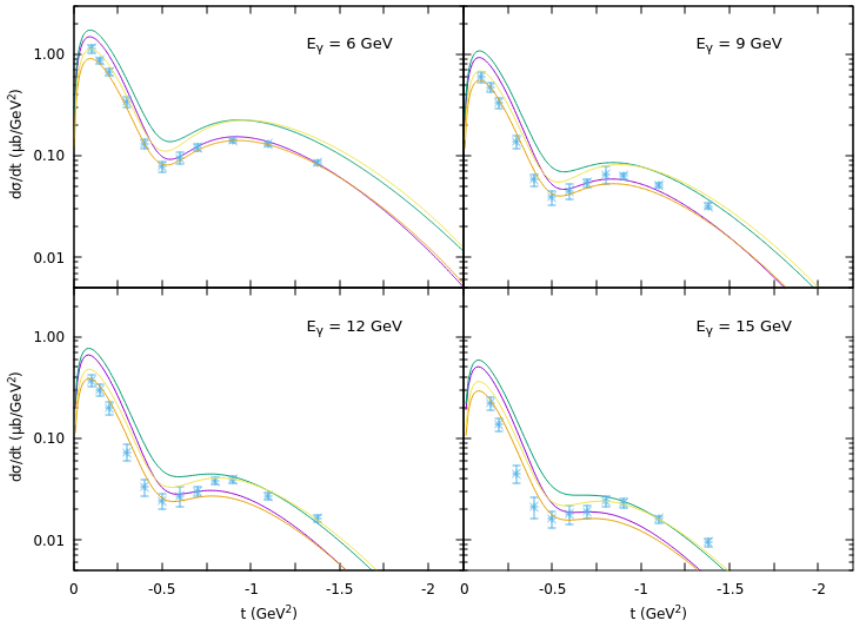


Figure 4.10: Illustration of the different Regge choices (parameters + scale) in the GLV model. GLV + dynamic scale (green), KM + dynamic scale (yellow), GLV + static scale (purple) and KM + static scale (orange). Data is from [38]

By comparing these curves a number of things can be learned. First of all we point out that for lower $|t|$ the different parameter sets give very different results, but at higher $|t|$ the importance of the trajectory parameter is a lot smaller compared to the scale used. By looking at the lower $|t|$ region across all diagrams we can rule out the GLV parameter set, as the KM parameters

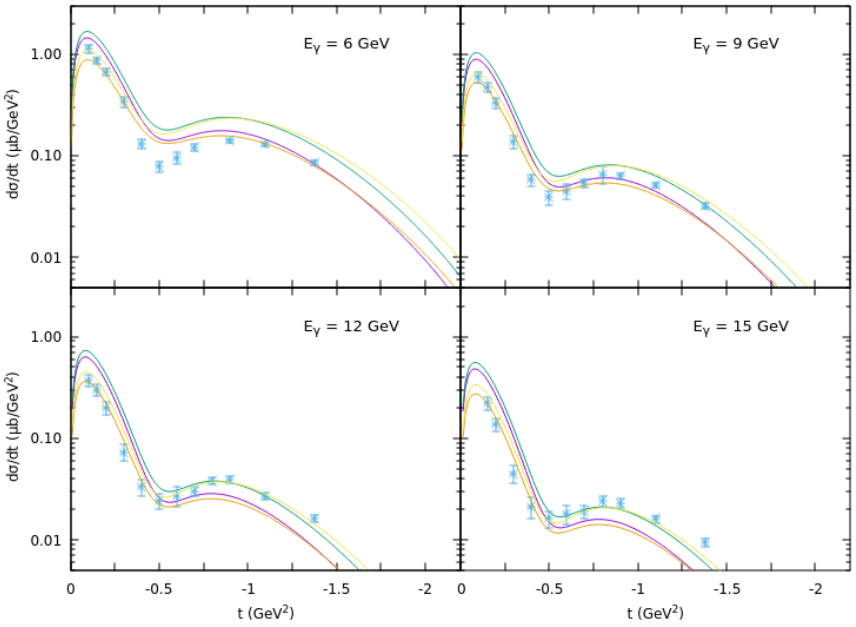


Figure 4.11: Illustration of the different Regge choices (parameters + scale) in the KM model. GLV + dynamic scale (green), KM + dynamic scale (yellow), GLV + static scale (purple) and KM + static scale (orange). Data is from [38]

clearly describe the data better. This is fortunate, as the KM trajectories are more recent and thus more precisely determined.

For the preferred scale we have to make a distinction between low and high $W$ (or $E_\gamma$). For low $W$ the preferred model is GLV. At low $|t|$ the dynamic scale is slightly better, while the static scale seems to win out at the higher end of the spectrum. At higher W values, both models give quite good results, but here we find the opposite as before. In the low $|t|$ region, the static scale is a better fit and at high $|t|$ the dynamic scale is favoured.

It is interesting to point out that this last observation, that the dynamic scale gives better predictions at the higher $E_\gamma$ and $|t|$, has also been found in charged pion production. A possible way to go forward could be combining the static and dynamic scales.

To summarize in this chapter we took the Reggeized Born term model and made it concrete, by specifying the different terms that would contribute to pion production reactions. We used this model to calculate photoproduction cross sections, both in the charged and neutral pion case. In general our model is qualitatively good, but it needs more work to be quantitatively precise. We have seen that there are some parameters we can tune, such as coupling constants, Regge trajectories and Regge scale, but only the last one is useful to us. Finally we found 2 models for the neutral pion case, each using slightly different

diagrams. For the photoproduction case, both have their merits, but we will return to a comparison in the next chapter, when we study electroproduction.

# Chapter 5

# Electroproduction

Now that we know our model is at least qualitatively useful at the $Q^2 = 0$ limit, we will try to generalize to $Q^2 > 0$, which means electron-induced pionproduction (or electroproduction). For this extension our primary references are [22] and [23]. They took the earlier work done by [21] and extended it to respectively charged pion electroproduction and neutral pion electroproduction off protons. They accomplished that by introducing $Q^2$-dependent form factors in the vertices $\gamma\pi X$, where $X$ is the exchanged particle. Furthermore they worked out a form factor for the nucleon channel that takes into account the effect of other high-mass (and spin) nucleon resonances. Instead of working with their expression for the nucleon form factor, which is quite complex in its functional form, we will use an alternate form factor proposed by [24]. Their work refined the model by [22], simplifying the nucleon form factor and reducing the number of parameters in the model. In the next section we will explicitly state the different changes we made to progress into $Q^2 > 0$ territory. After that we will look at both the charged pion and neutral pion results.

## 5.1 Methodology

The most obvious way of extending our model, and its diagrams, to $Q^2 > 0$ is by introducing transition form factors that depend on $Q^2$. For the $\gamma\pi X$ vertices (with $X$ the exchanged particle), we make use of the vector meson dominance model (VMD). That model states that when a photon interacts with a hadron it can be described as a vector meson interacting with that hadron. Though it was developed before QCD was accepted it is still useful to calculate transitional form factors for pions, which is precisely what we need.

VMD predicts that the form factor for these vertices is of a monopole form:

$$F_{\gamma\pi X} = \left(1 + \frac{Q^2}{\Lambda^2_{\gamma\pi X}}\right)^{-1}$$

The different $\Lambda$ we use as given by VMD are [22]: $\Lambda_{\gamma\pi\rho} = \Lambda_{\gamma\pi b_1} = m_\omega = 782$ MeV, $\Lambda_{\gamma\pi a_1} = m_\rho = 770$ MeV. For the $\omega$-channel, the relevant $\Lambda$ was obtained from a fit to data by [23] giving $\Lambda_{\gamma\pi\omega} = 1200$ MeV. The final transition form factor is for the pion t-channel exchange. In [22] use three different values for $\Lambda$, depending on $Q^2$ values. We will opt for the approach by [24] who used an average value $\Lambda_{\gamma\pi\pi} = 655$ MeV for the whole range and still got decent results. We will later show that these small differences in this parameter only have a limited effect on the cross section.

Introducing a $Q^2$-dependent transition form factor for the proton (in the nucleon channel) is a bit harder. A possible choice is the proton Dirac form factor

$$F_s(Q^2, s) = F_1^P(Q^2) \approx \left(1 + \frac{Q^2}{\Lambda^2_{\gamma pp}}\right)^{-2}$$

It is argued by [22] that such a form factor is insufficient as the exchanged proton could be highly off-shell. A possible way to remedy this is by taking into account higher mass, higher spin resonances of the exchanged nucleon. Essentially this is done by integrating the dipole transition form factors of the resonances, over the range of possible resonances. This is done in detail in [22], here we will show their result for the s-channel form factor:

$$F_s(Q^2, s) = \frac{\int_{M_P^2}^{\infty} ds_i \frac{s_i^{-\beta}}{s - s_i + i0^+} \left(\frac{1}{1+\xi\frac{Q^2}{s_i}}\right)^2}{\int_{M_P^2}^{\infty} ds_i \frac{s_i^{-\beta}}{s - s_i + i0^+}}$$

This expression already has 2 parameters, $\beta$ and $\xi$, that need to be fitted and the expression that follows from calculating the integral is quite terrifying.

An alternative approach is described by [24]. They argue first that the above form factor for $F_s$ is not correct for the on-shell limit. In this limit no resonances are expected and so the form factor should reduce back to the Dirac form factor. But when applying this they found that the form factor $F_s$ in [22] does not reduce correctly with the parameters given in that work. Instead they use this on-shell limit to constrain that form factor to a specific value of $\xi$. But they go even further, proposing a much more straightforward 'phenomenological' form factor:

$$F_s(Q^2, s) = \left(1 + \frac{Q^2}{\Lambda^{*2}_{\gamma pp}}\right)^{-2}$$

with

$$\Lambda^*_{\gamma pp}(s) = \Lambda_{\gamma pp} + (\Lambda_\infty - \Lambda_{\gamma pp})\left(1 - \frac{m_p^2}{s}\right)$$

and for the u-channel an analogue expression for $F_u(Q^2, u)$ with

$$\Lambda^*_{\gamma pp}(u) = \Lambda_{\gamma pp} + (\Lambda_\infty - \Lambda_{\gamma pp})\left(1 - \frac{m_p^2}{2m_p^2 - u}\right)$$

We will make use of this simpler form factor in the nucleon channel and the parameters derived in their fit to data, $\Lambda_\infty = 2194$ MeV and $\Lambda_{\gamma pp} = 840$ MeV.

A final change to the nucleon channel that is included here is an anti-shrinkage effect, by changing the slope of the pion trajectory in the s/u-diagrams:

$$\alpha'_\pi \to \frac{\alpha'_\pi}{1 + a\frac{Q^2}{s}}$$

with $a = 2.4$. Note that, just like all other changes we made for the extension to electroproduction, this effect disappears at the real photon point $Q^2 = 0$ so none of our previous results are impacted by them.

As a consequence of introducing $Q^2$-dependent with different form factors the pion t-channel diagram combined with the nucleon exchange diagrams are no longer gauge-invariant. To remedy this, we add an extra term into the current, which fixes gauge-invariance once more:

$$\mathcal{O}^\mu_{\pi,s} = \mathcal{I}\ g_{\pi NN}\gamma^5 \left( (F_{\gamma pp} - F_s)\frac{-Q^\mu}{Q^2} \right) (t - m_\pi^2)\mathcal{P}_{Regge}$$

where the isospin $\mathcal{I}$ is the same one as in the nucleon channel diagrams. For the u-channel there is a similar diagram but it has an overall minus sign compared to the one for the s-channel. It is important to point out here that the Regge propagator for $F_s$ uses the $Q^2$-dependent slope (as it comes from the nucleon exchange), while for the $F_{\gamma\pi\pi}$ we do not employ the $Q^2$-dependent slope (as it stems from the pion t-channel exchange).

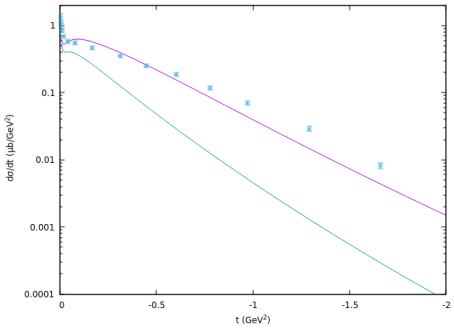


Figure 5.1: Illustration of the effect of $t$-dependent couplings (in green), compared to the original model (in purple) for photoproduction. This addition gives consistently worse results. Data is from [36]

Contrary to earlier modifications, which all disappeared in the real photon case, there is a proposal in [24]for a $t$-dependency of the coupling constants. They introduce a monopole factor in the coupling constants:

$$g_{xNN}(t) = g_{xNN}F_{m_x(t)}$$

and

$$F_{m_x}(t) = \left(1 + \frac{m_x^2 - t}{\Lambda_{m_x}^2}\right)$$

where $x$ stands for the 'ground state' particle of the Regge trajectory ($\pi$, $\rho$, ...). By amending the coupling constants in this fashion, they aim for a better description of the data at higher $|t|$, which is a problematic region for their model. But this change has its repercussions for the photoproduction case as well. We calculated these and found a systematically worse estimate of the photoproduction cross section, often by orders of magnitude. See figure 5.1 for an example of such a comparison. Therefore we have decided to not include this dependency on $t$ in our calculations.

## 5.2 Charged Pion results

There are two reactions covered by this section:

$$\gamma + p \to \pi^+ + n$$

and

$$\gamma + n \to \pi^- + p$$

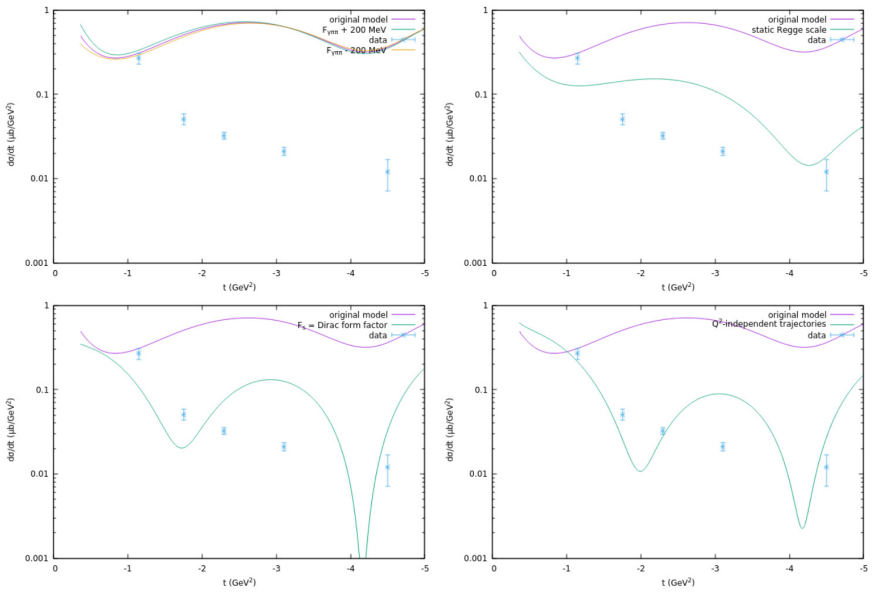


Figure 5.2: Comparison of cross sectional data ([39]) with our model for $W = 2.21$ GeV and $Q^2 = 3.85$ GeV$^2$. In addition, we have shown the impact of a number of 'alternative' models.

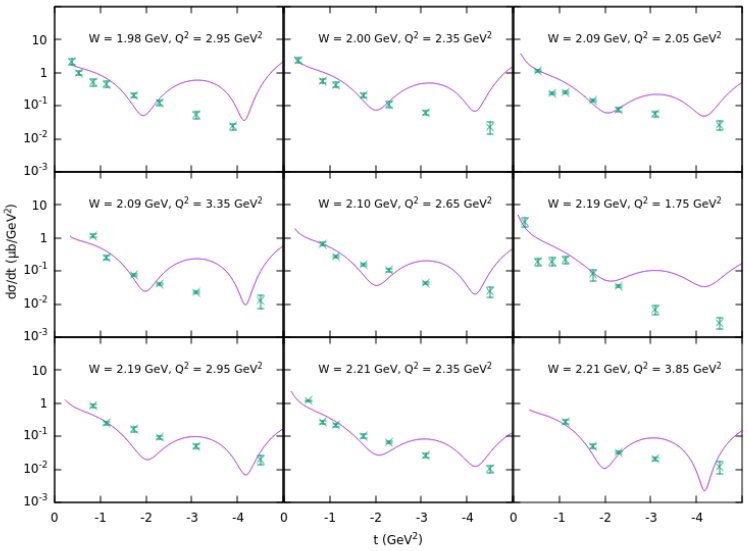


Figure 5.3: Comparison of cross sectional data ([39]) with the chosen model (see text) for different combinations of $W$ and $Q^2$. Notice the better agreement with data as $W$ increases and $Q^2$ decreases.

We will focus on the cross sections calculated for the $\pi^+$ experiment (as the $\pi^-$ computations are very similar). In figures 5.2 and 5.5 - 5.8 (which you can find in the subsection at the end of the discussion) we show the results along with a number of alternative models, where we made slight changes to our original model, in comparison to the data. We will discuss these in this section.

First we notice that our model is in general quite a bad description of the cross section data. Except for the lowest $|t|$ region, where the agreement is okay, it overestimates the data, sometimes by orders of magnitude, for $|t| > 1$ GeV$^2$. We can try to optimize our predictions by making small changes to the model, which we will do, but we have to stress that the same holds for electroproduction as for photoproduction: this model can describe the data qualitatively good at best, but for it to be quantitatively useful it needs more work.

In the upper left corners of the figures we show the effect of changing the pion exchange form factor, by adding or subtracting 200 MeV from $\Lambda_{\gamma\pi\pi} = 655$ MeV. We see that this changes the cross section only a little. So while it could be interesting for a more precise fit of very low $|t|$ data, it is not very useful for the high $|t|$ region. We have tried similar tweaks to the form factors for the $\rho$ and $a_1$ and have found a similar behavior, though less pronounced than for the $\pi$.

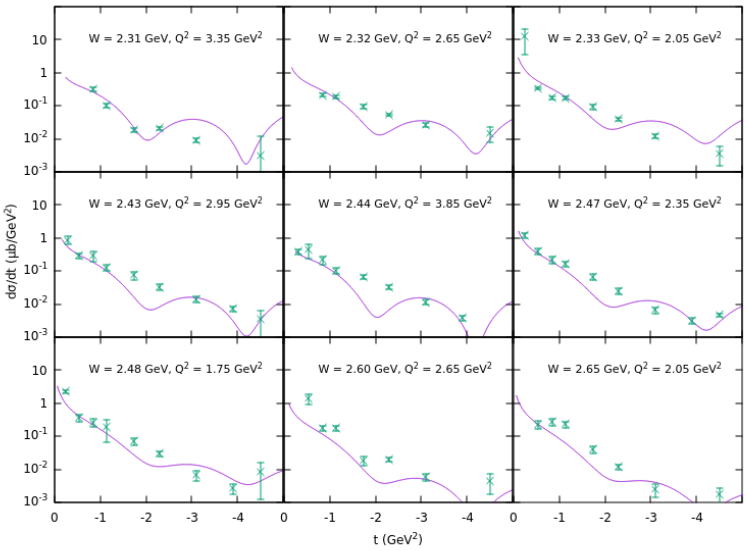


Figure 5.4: Comparison of cross sectional data ([39]) with the chosen model (see text) for different combinations of $W$ and $Q^2$.

For that reason we have left these out of our figures.

In the upper right corner we have chosen a static Regge scale, which means that instead of scaling $s$ like $\alpha' s$ in the Regge propagator, we use the fixed value $s/1$ GeV$^2$. This change lowers the cross section by quite a bit in the higher $|t|$ range, though the predicted cross section falls too slow to explain the data, in particular for lower $W$.

In the lower left corner we changed the proton transition form factor to the classic dipole factor. From physical principles alone, it seems strange to go back to the simpler form factor, but we will do it to see if we can simplify our calculations. The dipole form factor has a drastic effect on the cross section and it drops down until it comes closer to the data.

We notice something similar when we do not use the $Q^2$-dependent nucleon channels (lower right corner), opting instead for the fixed trajectories, like we used in photoproduction. The cross section we find lies a lot lower as well, coming much closer to the data than in our original model.

There are some more general remarks to be made about our results. First, we seem to have better overall agreement with the data (over all the alternative models) when looking at lower $Q^2$ and higher $W$. This is not surprising, as Regge theory is only valid at high $W$ and because we approximate all reactions as hadronic instead of partonic, we expect that our description is worse for

higher $Q^2$.

Furthermore there is a clear difference between the higher and lower $Q^2$ fits. In higher $Q^2$ calculations, there is the appearance of several huge dips in the cross section, which we don't find at all in the data. We have not find what causes these dips to appear, but notice that they show up at slightly different places for different alternative models.

Finally, to illustrate more clearly the range of $W$ and $Q^2$ we show the results for the model without the $Q^2$-dependent trajectories for a number of different $W/Q^2$ combinations in figures 5.3 - 5.4. We have chosen $Q^2$-independent trajectories as that change seems to describe the data the best, though we have to admit that the difference with the model that includes the Dirac form factor is not very big.

### 5.2.1 Extra figures

These are some extra figures for the cross section of electroproduction compared to the data, for several $W$ and $Q^2$ combinations. Remember that the upper left corner describes the influence of a change in the value of the transition form factor parameters. The upper right corner compares the different scalings of $s$ in the Regge propagator. The lower left corner compares to a simpler Dirac form for the nucleon form factor. Finally the lower right corner shows the influence of the $Q^2$-dependence in the nucleon Regge trajectories.

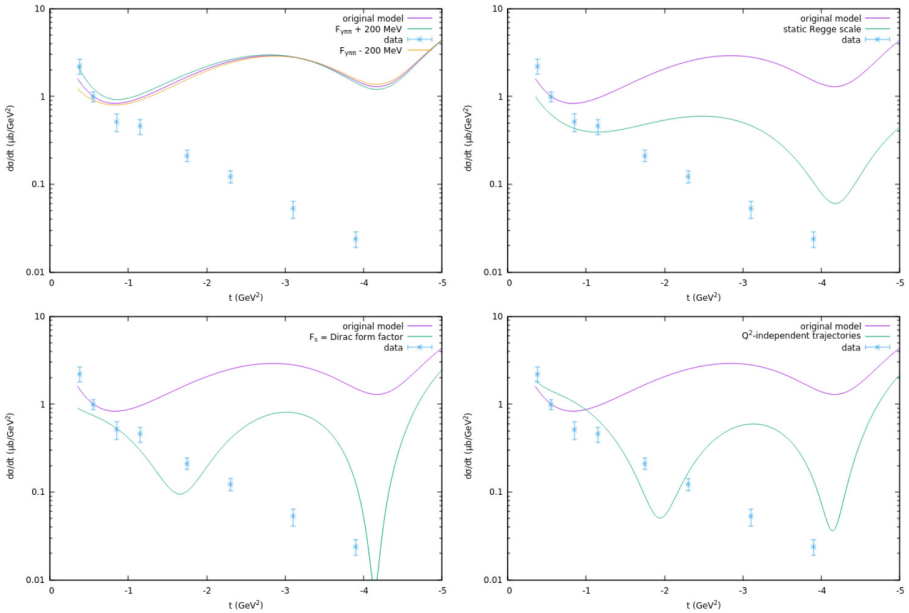


Figure 5.5: Comparison of cross sectional data ([39]) with our model for $W = 1.98$ GeV and $Q^2 = 2.95$ GeV$^2$. In addition, we have shown the impact of a number of 'alternative' models.

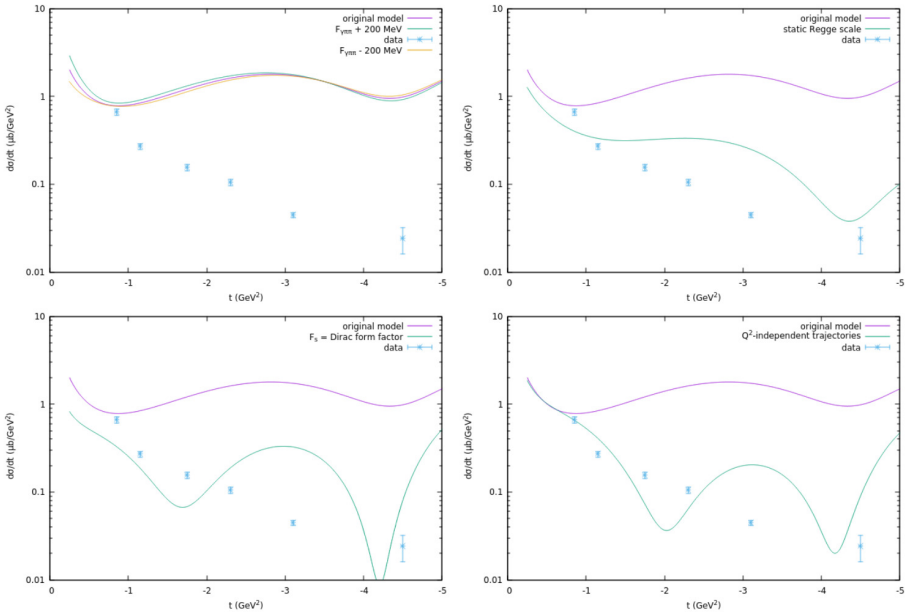


Figure 5.6: Comparison of cross sectional data ([39]) with our model for $W = 2.10$ GeV and $Q^2 = 2.65$ GeV$^2$. In addition, we have shown the impact of a number of 'alternative' models.

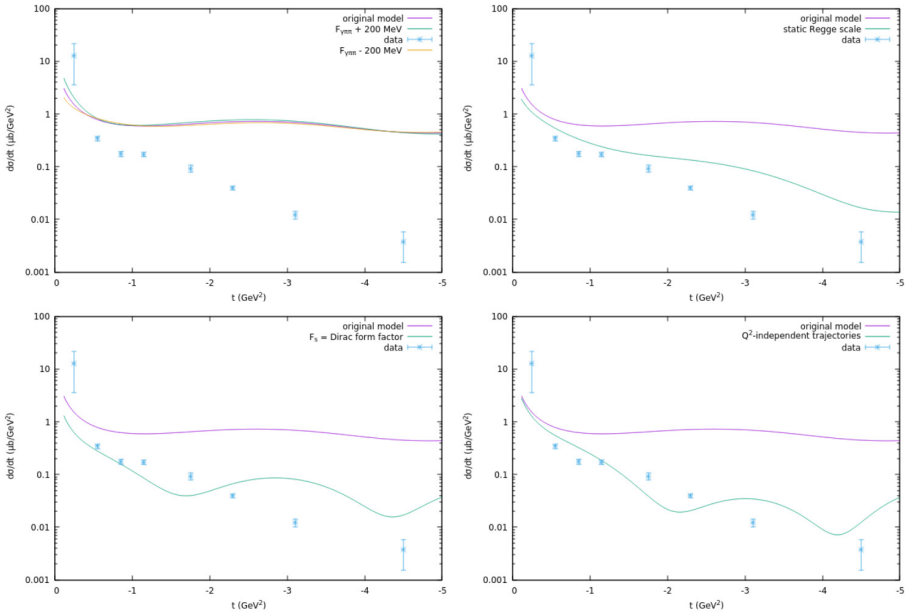


Figure 5.7: Comparison of cross sectional data ([39]) with our model for $W = 2.33$ GeV and $Q^2 = 2.05$ GeV$^2$. In addition, we have shown the impact of a number of 'alternative' models.

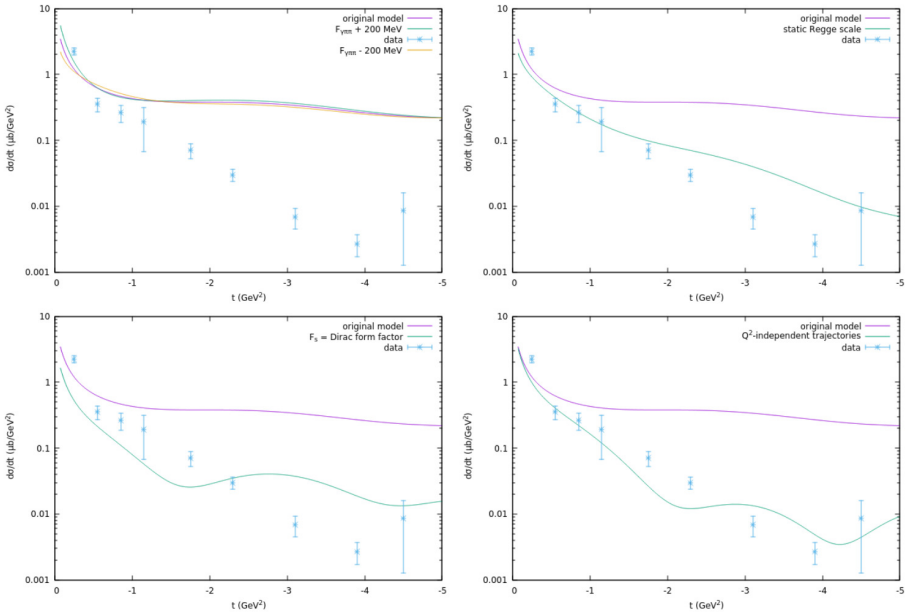


Figure 5.8: Comparison of cross sectional data ([39]) with our model for $W = 2.48$ GeV and $Q^2 = 1.75$ GeV$^2$. In addition, we have shown the impact of a number of 'alternative' models.

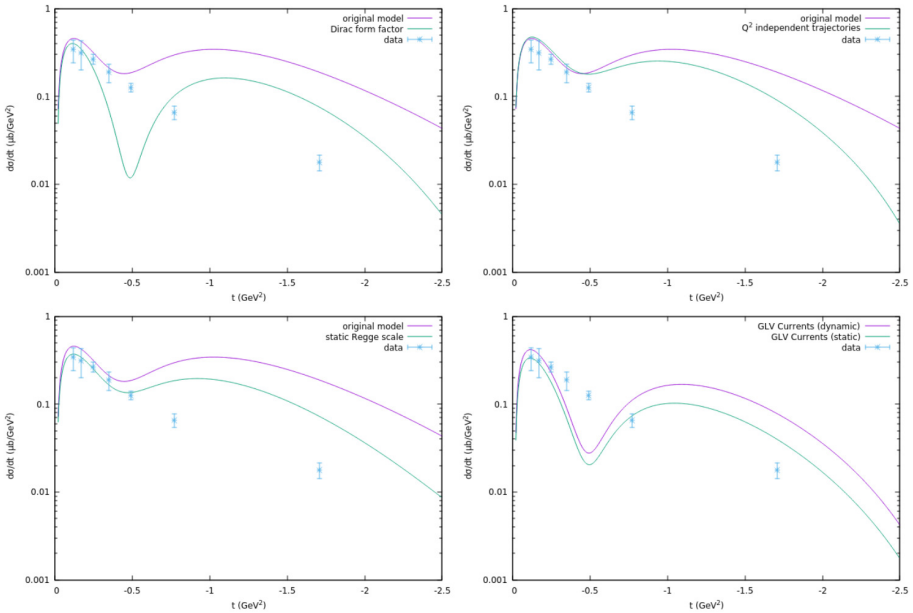


Figure 5.9: Comparison of cross sectional data ([40]) with our model for $W = 2.91$ GeV and $Q^2 = 1.15$ GeV$^2$. In addition, we have shown the impact of a number of 'alternative' models.

## 5.3 Neutral Pion results

There are two reactions we will discuss:

$$\gamma + p \to \pi^0 + n$$

and

$$\gamma + n \to \pi^0 + n$$

The focus in this section, is again on the proton reaction, for similar reasons as explained in the photoproduction chapter.

For the neutral pion production, there is the big difference that we have 2 'main' models, meaning we have 2 models (GLV and KM) with slightly different diagrams as discussed in the chapter on photoproduction. In the first one there is no nucleon channel, which means the possibility to mess with the proton transition form factor or to have $Q^2$-dependent Regge trajectories is no option. In the other model, these tweaks are possible.

In the figures 5.9 and 5.12 - 5.14 (which you can find in the subsection at the end of the dicussion) we show the cross sections computed by the 2 main models, along with a number of alternative models (where we made small changes to the original model) and compared them to available data.

We will begin by discussing the first 'main model', the KM model, which is the model by [23], which has its results depicted in the 2 upper and the lower left plots each figure. For a start, we see that it describes the data reasonably well at the lower end of the $|t|$ spectrum ($|t|0.5$ GeV$^2$) but fails spectacularly to reproduce the decrease seen in the data at higher $|t|$. Just like in the charged pion case, the original model is not good enough without some changes.

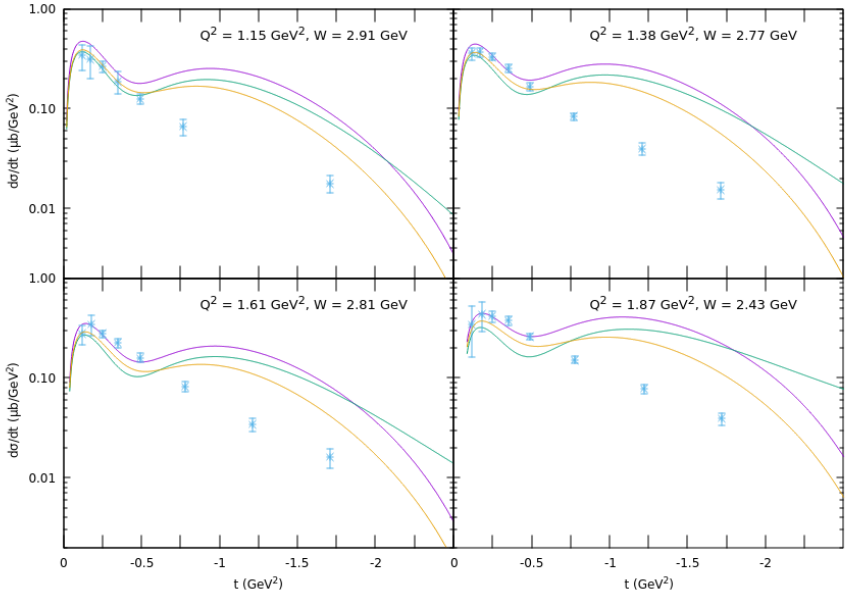


Figure 5.10: Comparison of cross sectional data ([40]) with the chosen model (see text) for different combinations of $W$ and $Q^2$. Notice the better agreement with data as $W$ increases and $Q^2$ decreases.

When we look at the second 'main model', the GLV model[21], and even its alternative with a static scale for $s$ in the Regge propagator, we find that they are also flawed in their description of the data and it is arguably worse. For the lower $|t|$ data the model suffices only for the lowest $Q^2$ but breaks down at any higher values. The cross sections found have these large dips at $t \approx -0.5$ GeV$^2$ and these are not seen at all in the data. The higher $|t|$ range is somewhat better but it still is not great. We will see, in the coming discussion, that changes to the first model can produce similar high $|t|$ behavior without having the drawback of the bad predictions at low $|t|$. Therefore we won't look further into the second model in this work. It could be that it works better in other ranges of $Q^2$ and $W$ for electroproduction, but at this point that is not suggested in our results.

Now coming back to the first model, there are some changes we can propose, in line with the charged pion case. We will not tinker with the values of the form factor parameters, as we saw previously that their effect is quite limited, so we suspect that they will also not help us in this case. We do try to change

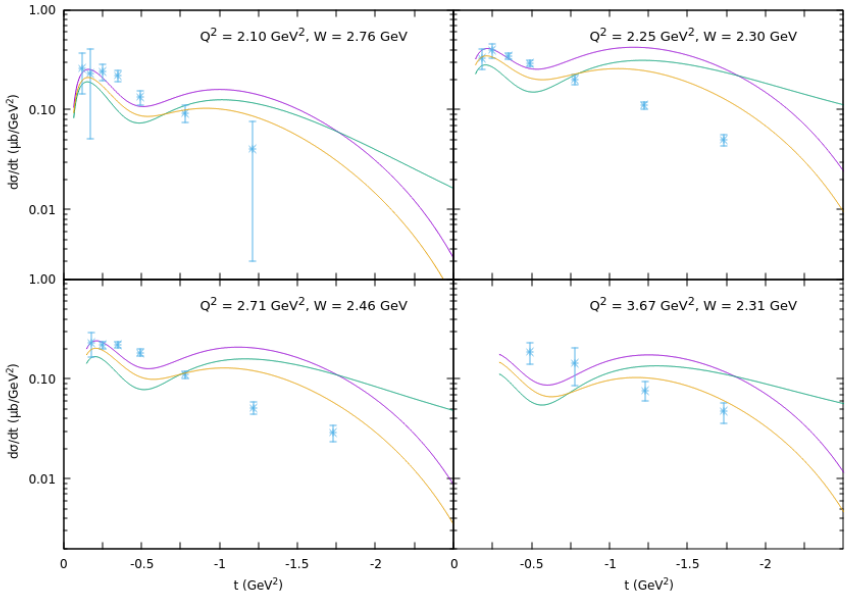


Figure 5.11: Comparison of cross sectional data ([40]) with the chosen model (see text) for different combinations of $W$ and $Q^2$. Notice the better agreement with data as $W$ increases and $Q^2$ decreases.

the proton form factor in the Dirac form factor, illustrated in the upper left corner of the figures. The result is not too hopeful. While for higher $|t|$ the curves is lowered, there is the introduction of a dip at $t \approx -0.5$ GeV$^2$, which worsens the good match we found earlier for lower $|t|$. So while the Dirac form factor did provide us with better results for charged pion production, it is not at all useful for neutron pion production, so we conclude it is best to not keep it around, in all cases. We can confirm that the work done to find a better proton form factor [22][24] has proven useful to our calculations.

Now there are two changes left that both have their merit. In the upper right corner we try the original Regge trajectory for the nucleon channel, without any $Q^2$ dependence, and in the lower left corner we compared to a model with a static Regge scale ($s/1$ GeV$^2$). In both cases we see a decline in the cross section at higher $|t|$ that comes closer to the data than we had before. For the independent Regge trajectories there is also an even better match with the cross sectional data at the lower end of the $|t|$ spectrum, which is remarkable as the agreement was already pretty good. Notice that in the charged pion case, these two changes also improved our calculations, which makes us suspect that these might be necessary additions for our model to function more correctly.

Recall that in the case of neutral pion photoproduction we found for 'lower' $W$ (which is the case for all our calculations in this section) that the dynamic scale should be a better description of the data at lower $|t|$ while the static

scale is preferred in the higher $|t|$ section. To accurately check if this still holds for electroproduction, we have to compare static and dynamic scale for a given model. In figures 5.10 - 5.11 we compare the data with the two alternative models that gave the best results, static scale and $Q^2$-independent trajectories, and also introduce a model that combines the two. This means we can compare the static and dynamic scale for $Q^2$-independent trajectories. These results seem to generally agree with our earlier observations: the static scale, while still overestimating the data, is closer again than the dynamic scale for $t < -0.5$ GeV$^2$, while for most of the modelled reactions the dynamic scale seems slightly better in the forward region.

A final more general remark is that our model is in better agreement with the data as $W$ increases and $Q^2$ decreases, which is completely in line with the region where this model is supposed to work best.

In this chapter we introduced some recipes to implement the $Q^2$-dependence for the electroproduction process. While we found an overall good qualitative agreement with the data for photoproduction, there was more difficulty in getting the electroproduction predictions right. Initially our Reggeized Born term model was bad at reproducing the data and we have examined multiple tweaks to our model to make our predictions better match with experiment. From these changes we can conclude that the off-shell form factor for the nucleon channel is needed to describe the data (especially in the neutral pion case) and that the agreement is much better without $Q^2$-dependent Regge trajectories. Additionally the neutral pion model with the nucleon channels[23] is definitely better suited for electroproduction than the one without[21]. Finally we note that the values of $W$ we looked at were a lot lower than for photoproduction, while the $Q^2$ was relatively high, which could mean we are getting to the edge of where hadronic physics holds. These last observations could be an additional explanation of the worse match with the data.

### 5.3.1 Extra figures

These are some extra figures for the cross section of electroproduction compared to the data, for several $W$ and $Q^2$ combinations. Remember that the upper right corner compares our model to a simpler Dirac form for the nucleon form factor. The lower right corner shows the influence of the $Q^2$-dependence in the nucleon Regge trajectories.The lower left corner compares the different scalings of $s$ in the Regge propagator. Finally the lower right depicts the GLV model with both scaling options.

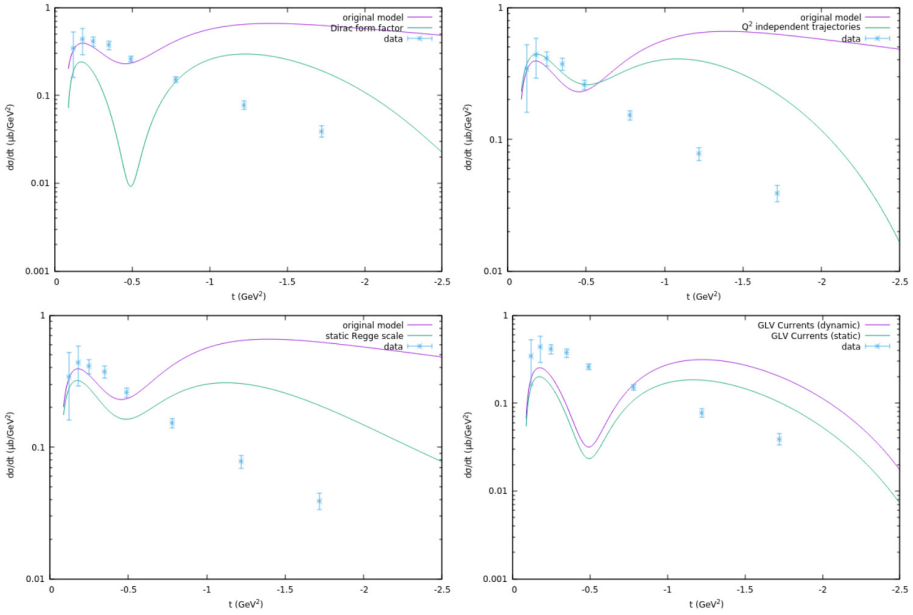


Figure 5.12: Comparison of cross sectional data ([40]) with our model for $W = 2.43$ GeV and $Q^2 = 1.87$ GeV$^2$. In addition, we have shown the impact of a number of 'alternative' models.

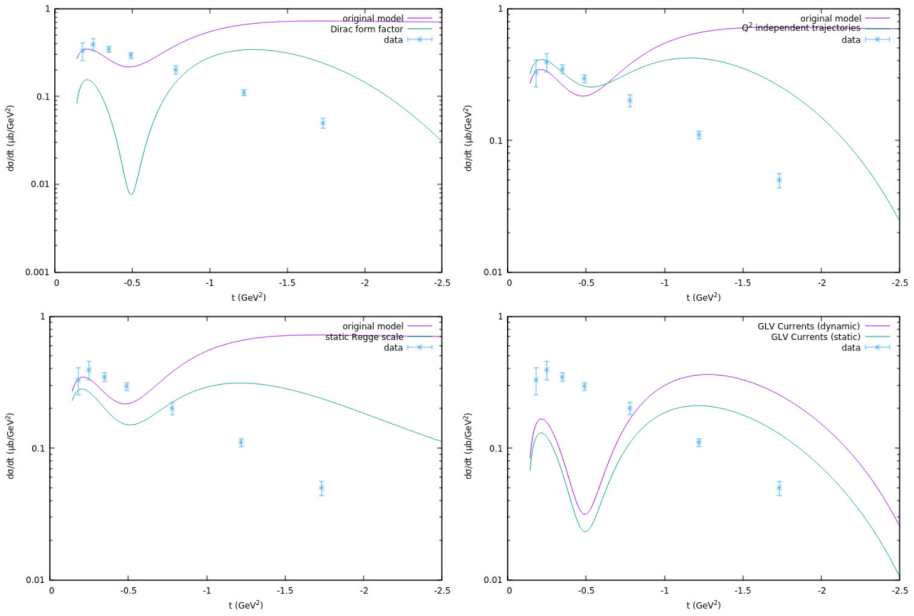


Figure 5.13: Comparison of cross sectional data ([40]) with our model for $W = 2.30$ GeV and $Q^2 = 2.25$ GeV$^2$. In addition, we have shown the impact of a number of 'alternative' models.

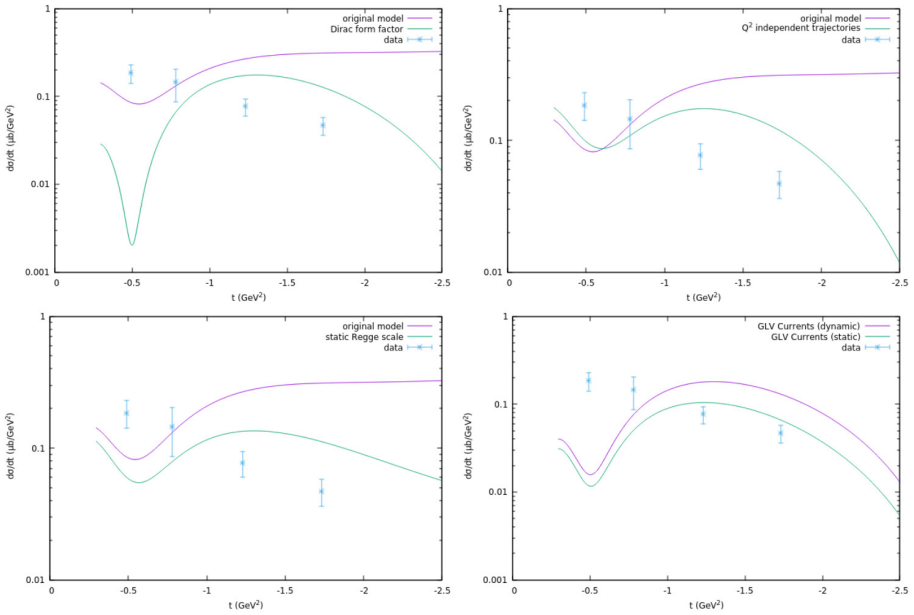


Figure 5.14: Comparison of cross sectional data ([40]) with our model for $W = 2.31$ GeV and $Q^2 = 3.67$ GeV$^2$. In addition, we have shown the impact of a number of 'alternative' models.

# Chapter 6

# Neutrinoproduction

To extend the models we previously used into neutrinoproduction territory, we have referred to several works that have extended their models to work for neutrinos. In [20], a SPP Regge model is worked out based on the low energy Chiral Perturbation Theory background diagrams. They also include an extension to neutrinoproduction, both for the charged and the weak current. Ref. [42] also works out their diagrams in more detail, especially concerning the isospin relations.

First for the vector current, the derived diagrams for electroproduction can be reused for ceak interactions, by a property called conserved vector current (CVC). The electromagnetic current consists of a isoscalar and a isovector part. CVC states that the isovector current of the EM current and the weak isovector current are both just different components of the same isospin current. As a consequence of this relation we can use the same diagrams for the CC vector current as we derived in the electroproduction case, with the same form factors and couplings.

For the axial current we can use a similar property, partial conservation of axial current (PCAC), to link the divergence of the axial current to the $\pi N$ diagram, which gives us the relevant t-channel exchange diagram. This is done in [41].

One of the difficulties associated with neutrinoproduction is the lack of experimental data, especially compared to the plethora of photo- and electron-production data. We will look at a paper that presents the result of exclusive SPP from neutrinos and antineutrinos in a broad energy range [43]. Instead of providing us with cross sections, it states the number of neutrino events, so we will have to normalize our results. We can specifically test the axial current by comparing it to the elastic $\pi N$ channel cross sections [45]. We are able to do this by caculating a specific structure function that can be related to both the axial current and the elastic scattering cross section [41][44].

## 6.1 Charged Current

### 6.1.1 Methodology

#### Vector Current

The most straightforward extension from electroproduction to neutrinoproduction is to focus on the vector current first. We will do it separately for the charged current and neutral current neutrino reations.

The first question to ask about charged current (CC) neutrinoproduction is what diagrams contribute to which reactions. The exchanged boson ($W^{\pm}$) now carries electric charge, so the exchanged Regge trajectory will have zero charge in the case of charged pion CC neutrinoproduction and non-zero charge in the case of neutral pion CC neutrinoproduction. This means we will use the charged pion diagrams in the neutral pion CC case and vice-versa.

As we explained above it is by making use of CVC that we can just take over the EM currents and use them here, with all the same form factors and couplings. As a consequence we find the following relation between the matrix elements: [42]

$$\langle \pi^+ p|\mathcal{J}^V_{CC}|p\rangle = \cos(\theta_C)(\sqrt{2}\,\langle \pi^0 n|\mathcal{J}_{EM}|n\rangle + \langle \pi^- p|\mathcal{J}_{EM}|n\rangle$$

$$\langle \pi^+ n|\mathcal{J}^V_{CC}|n\rangle = \cos(\theta_C)(\sqrt{2}\,\langle \pi^0 p|\mathcal{J}_{EM}|p\rangle - \langle \pi^- p|\mathcal{J}_{EM}|n\rangle$$

The matrix elements for the other reactions are related to the matrix elements above by making use of the Wigner-Eckhart theorem. This gives us the following relations:

$$\langle \pi^- n|\mathcal{J}^V_{CC}|n\rangle = \langle \pi^+ p|\mathcal{J}^V_{CC}|p\rangle$$

$$\langle \pi^- p|\mathcal{J}^V_{CC}|p\rangle = \langle \pi^+ n|\mathcal{J}^V_{CC}|n\rangle$$

$$\langle \pi^0 n|\mathcal{J}^V_{CC}|p\rangle = -\langle \pi^0 p|\mathcal{J}^V_{CC}|n\rangle = \frac{1}{\sqrt{2}}(\langle \pi^+ p|\mathcal{J}^V_{CC}|p\rangle - \langle \pi^+ n|\mathcal{J}^V_{CC}|n\rangle)$$

We absorb the factor $\cos(\theta_C)$ in the kinematics. Before we state the exact isospin values we point out that for the rho current the isospin current for any CC reaction is zero, so the rho diagram does not contribute to the vector current part of the CC cross section. For the other diagrams we have the following values:

| | $\pi t - channel$ | s-channel | u-channel | $\omega t - channel$ |
|---|---|---|---|---|
| $W^+ + p \to \pi^+ + p$ | $-\sqrt{2}i$ | 0 | $-\sqrt{2}i$ | $\sqrt{2}$ |
| $W^+ + n \to \pi^+ + n$ | $\sqrt{2}i$ | $-\sqrt{2}i$ | 0 | $\sqrt{2}$ |
| $W^- + p \to \pi^- + p$ | $\sqrt{2}i$ | $-\sqrt{2}i$ | 0 | $\sqrt{2}$ |
| $W^- + n \to \pi^- + n$ | $-\sqrt{2}i$ | 0 | $-\sqrt{2}i$ | $\sqrt{2}$ |
| $W^+ + n \to \pi^0 + p$ | $2i$ | $-i$ | $i$ | 0 |
| $W^- + p \to \pi^0 + n$ | $-2i$ | $i$ | $-i$ | 0 |

Two final remarks before we move on from isospin. The isospin values for the omega exchange show more explicitly that the diagrams for charged pion CC are those of neutral pion NC and vice-versa. The omega exchange disappears (zero isospin) for neutral pion CC similar to charged pion NC having no omega exchange diagrams. Furthermore notice that the pion t-channel is now included in charged pion CC, while it was forbidden in the EM reactions. This is not surprising when you looking at the allowed vertex terms [20]. The neutral bosons (photon or Z-boson) do not couple to neutral pions, which is why there is no pion t-channel for NC/EM, but the W-bosons have vertices like $W^+ \to \pi^0\pi^+$ so the t-channel term is allowed for the charged pion CC case.

**Axial Current**

With the vector current done we turn to the axial current. We get the procedure on deriving the axial current diagram from the construction of the axial current in Chiral Perturbation Theory. In chiral theories, the result of a spontaneously broken chiral symmetry is a relation called 'partial conservation of axial current' (PCAC). For more details we refer to the original paper by M. Gell-Mann and M. Lévy [46], but in short it states that the divergence of the axial current is proportional to the pion field. This provides us with a recipe to derive the relevant axial currents. Beginning with a matrix element of the process $\pi + N \to m + b$, where m stands for meson and b for baryon, we replace the momentum of the incoming pion $k_\pi^\mu$ with $if_\pi\epsilon^\mu$ with $\epsilon^\mu$ the polarization vector for the external axial current and the pion decay constant $f_\pi = 93$ MeV. We can use this procedure to get the axial current for both the rho exchange and the nucleon channel diagram.

This has been worked out by [41] and here we will state the derived axial currents that can be used in our model:

$$\mathcal{O}^\mu_{s,A} = -\mathcal{I}\frac{g_A}{2}\frac{g_{\pi NN}}{2M}G_A(Q^2)\pi\gamma^5\frac{\not{p}_s + m_N}{s - m_N^2}\left(\gamma^\mu\gamma^5 + \frac{\not{Q}}{m_\pi^2 - Q^2}Q^\mu\gamma^5\right)$$

for the axial s-channel current,

$$\mathcal{O}^\mu_{u,A} = -\mathcal{I}\frac{g_A}{2}\frac{g_{\pi NN}}{2M}G_A(Q^2)\left(\gamma^\mu\gamma^5 + \frac{\not{Q}}{m_\pi^2 - Q^2}Q^\mu\gamma^5\right)\frac{\not{p}_u + m_N}{u - m_N^2}\pi\gamma^5$$

for the axial u-channel current, and

$$\mathcal{O}^\mu_{\rho,A} = \mathcal{I}f_\pi g_{\rho NN}g_{\rho\pi\pi}F_A(Q^2)\frac{1}{t - m_\rho^2}\left[\gamma^\mu - \frac{\kappa_\rho}{4m_N}(\gamma^\mu\not{q} - \not{q}\gamma^\mu)\right]$$

for the axial rho t-exchange current. The coupling constant $g_{\rho\pi\pi} = 6.938$ is a remnant of the way in which we derived the axial current, where we related the axial current by a pion (and so we have an effective $\rho\pi\pi$ vertex). In addition there is the axial current coupling constant $g_A = 1.26$.

For reasons we will explain later we have left out the Regge part, so these are the low energy currents.

For the isospin factors, we have worked them out in the same way as before. For the nucleon channel we end up with the same isospin as in the vector nucleon channel, which is obvious as we are looking at the same diagrams as before. Notice that there is an extra minus sign in front of our axial nucleon channels. This can be related back to the structure of the total weak current, which is a V-A (Vector minus Axial) structure. For the rho channel isospin we do a similar calculation and end up with the opposite isospin as in the pion t-channel diagrams (see table in the previous section).

The final components of these axial diagrams are the axial form factors. The axial transition form factor $F_A(Q^2)$ is similar to earlier transition form factors in the $\gamma\pi x$ vertices, but now instead of replacing the boson by a vector meson, we need an axial meson. The off-shell axial form factor $G_A(Q^2)$ was inspired by our off-shell proton form factor. and therefore has a very similar structure, but different values of parameters. These are

$$F_A(Q^2) = \frac{1}{1 + \frac{Q^2}{\Lambda_\rho^2}}$$

$$G_A(Q^2, s) = \left(1 + \frac{Q^2}{\Lambda_{Apn}^{*2}}\right)^{-2}$$

with

$$\Lambda_{Apn}^*(s) = \Lambda_{Apn} + (\Lambda_\infty^A - \Lambda_{Apn})\left(1 - \frac{m_p^2}{s}\right)$$

and for the u-channel an analogue expression for $F_u(Q^2, u)$ with

$$\Lambda_{Apn}^*(u) = \Lambda_{Apn} + (\Lambda_\infty^A - \Lambda_{Apn})\left(1 - \frac{m_p^2}{2m_p^2 - u}\right)$$

The parameters in these expressions are taken from [20] and have values: $\Lambda_\rho = 1260$ MeV, $\Lambda_{Apn} = 1050$ MeV and $\Lambda_\infty^A = 7200$ MeV. It is important to point out that these values have been found from a fit to the data, but with a different model than ours. In principle we should fit them again, but we choose to take them over here as we will, in the next section, first try to constrain the $Q^2 = 0$ limit before we look into the $Q^2$-dependence. As we will point out in the coming paragraphs, the $Q^2 = 0$ limit is clearly lacking, so it needs more work before adjusting the parameters in the $Q^2$-dependent form factors.

### 6.1.2 Results

One of the choices we can make is in deciding which axial currents we take into our model. The t-exchange rho is a must, as it is the only meson that contributes in the t-channel for the axial current. But a priori there is no requirement to take the s/u-channel exchanges into account. Unlike the pion t-channel diagrams, the rho diagram is gauge invariant on its own, so it does not

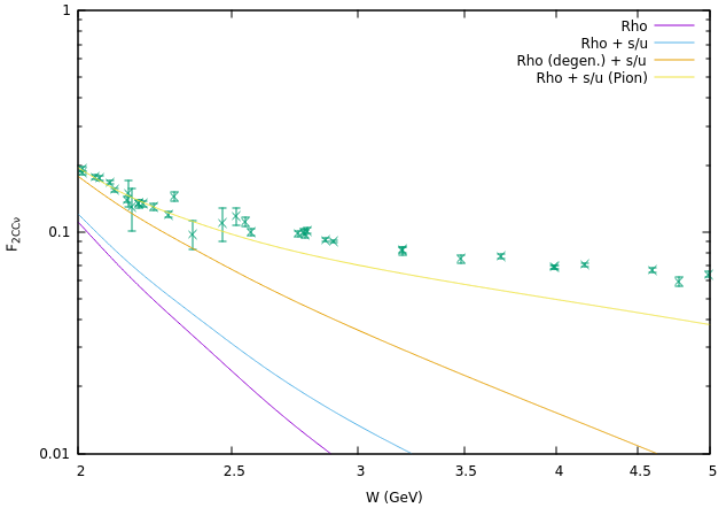


Figure 6.1: The structure function $F_2$ from data [45] compared to different versions of our model: rho exchange alone, rho + s/u exchange, rho + s/u with degenerate rho phase and rho + s/u with a pion propagator in the nucleon channel. This is for the reaction $\nu + p \to e + \pi^+ + p$.

need the nucleon exchange diagrams. In ref [20] the nucleon diagrams are added and they are reggeized with the same propagator as the rho exchange diagram, as the propagating meson for the axial current is the rho meson. Checking our axial current with the available data therefore seems like an important first before we start computing the combined (vector and axial) cross section.

One way to compare the results from our axial currents to experimental data is by calculating a structure function. At $Q^2 = 0$ the structure function $F_2$ of the neutrino induced interaction equals the same structure function in the pion nucleon elastic scattering reaction [44], due to Partially Conserved Axial Current (PCAC). In particular we can find experimental elastic scattering data [45] and relate them to the structure function by:

$$F_2 = \omega W_2 = \frac{2f_\pi^2}{\pi}\sigma(\pi N \to \pi N)$$

Then we calculate the differential cross section in our model and use it to compute the structure function as for $Q^2 = 0$

$$\frac{d^3\sigma}{dE_l' d\Omega'} = \frac{G_F^2 E_l'^2}{2\pi^2\omega} F_2$$

In figures 6.1 and 6.2 make a comparison between the experimental structure function and several possible axial currents. First we find that the axial rho current on its own does not suffice to explain the structure function. This is an

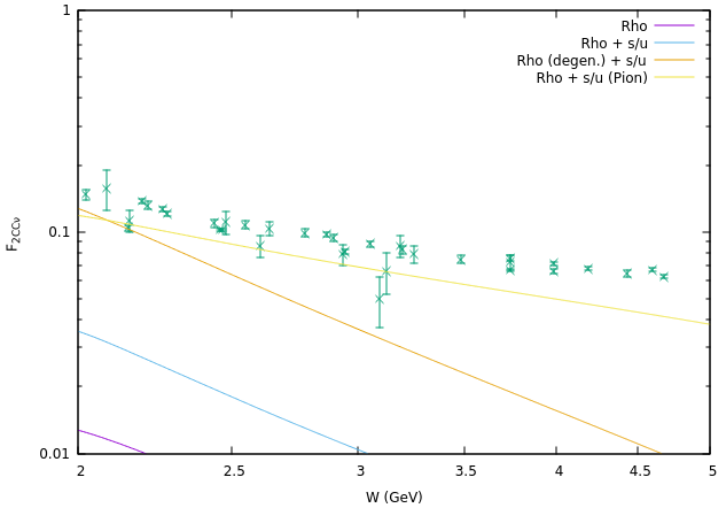


Figure 6.2: The structure function $F_2$ from data [45] compared to different versions of our model: rho exchange alone, rho + s/u exchange, rho + s/u with degenerate rho phase and rho + s/u with a pion propagator in the nucleon channel. This is for the reaction $\bar{\nu} + p \to e^+ + \pi^- + p$.

important observation, as it means the data needs the axial nucleon exchange channels to reproduce the data. Furthermore we have shown the influence of Regge phase for the rho propagator, by changing the phase we had in the KM model vector current to a degenerate phase. Changing the phase has a clear impact on the structure function, and the degenerate phase seems the preferred phase when comparing to the data.

Finally we have tried a pion Regge propagator for the nucleon channel (like we did in the vector current). The idea to try this came from how we reggeized the pion exchange earlier: it always consisted of a t-channel pion together with the s/u channel nucleon exchanges. We reggeize that sum with a pion Regge propagator and we could argue that, while the t-channel pion exchange does not contribute to the axial current, the nucleon channels do get an axial part. So we take that axial part of the nucleon exchange as a part of the combined pion exchange, which we give a pion Regge propagator. We have found that this describes the experimental structure function better than our earlier efforts.

We have to admit this is strange. Although we could make an argument for why the pion propagator could be there, the more obvious choice is still the rho propagator, as it is the only contributing meson to the axial current. Besides reggeizing the nucleon channel, which we remind does not need to be added, we could choose a whole other diagram. Other references, such as [47] point to a dominant pomeron (another Regge trajectory) exchange when describing $\pi N$ elastic scattering. In any case it is clear that the axial current needs further work and we will not conclusively find the right form in this thesis. A possible

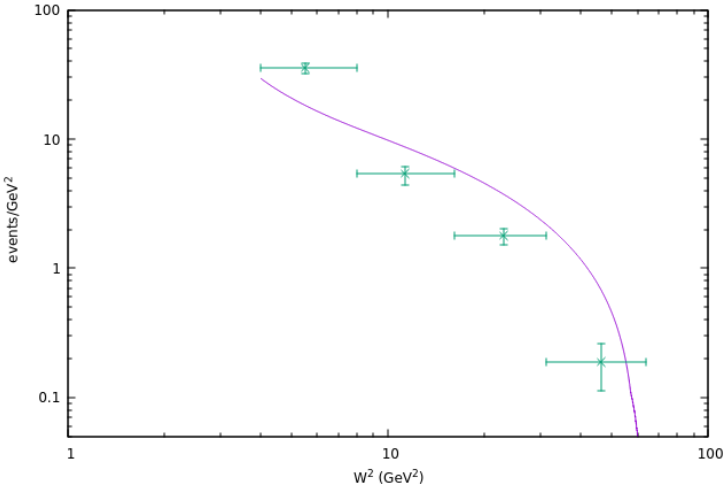


Figure 6.3: Scattering events as a function of $W^2$, with our model compared to data from [43]. The pion Regge propagator is used in the s/u-channel diagram.

avenue for further research is looking at the $t$-behavior of the model compared to elastic $\pi N$ data. For the structure function we depict here a integration over the $t$-range was done, so our results could have been influenced by the high $|t|$ region where our model is not as good as in the lower $|t|$. By observing the $t$-dependence such a bad influence is not possible and more constraints could be placed on a possible model.

Now we take a look at data for the combined current. Contrary to electro- and photoproduction the cross sectional data for SPP induced by neutrinos is rather limited. The first of our data sets comes from [43], a 1986 study which studies exactly this reaction for a big neutrino energy range. Besides the fact that the neutrino flux is quite broad, there are not a lot of details on the kinematics in their paper. Therefore we have chosen their average neutrino energy, $E_\nu = 32.6$ GeV, as an arbitrary high energy. A check at even higher energies showed us that the dependence on the energy is not relevant for our plots.

The data in this paper is expressed in number of events, so we had to take some care in normalizing our cross sections correctly. We performed this normalization by first integrating the cross section and then dividing each cross section by the total integrated cross section and then multiplying by the total number of measured events. The integration of the cross section is approximated by multiplying the cross section with $\Delta x$ (which is in our case either $\Delta t$ or $\Delta(W^2)$) and adding that over the whole $x$-range.

Because of this normalization only the trend in the cross section can be observed and we have no clue if the order of magnitude of the calculated cross section corresponds to reality. In the following figure we have chosen the pion

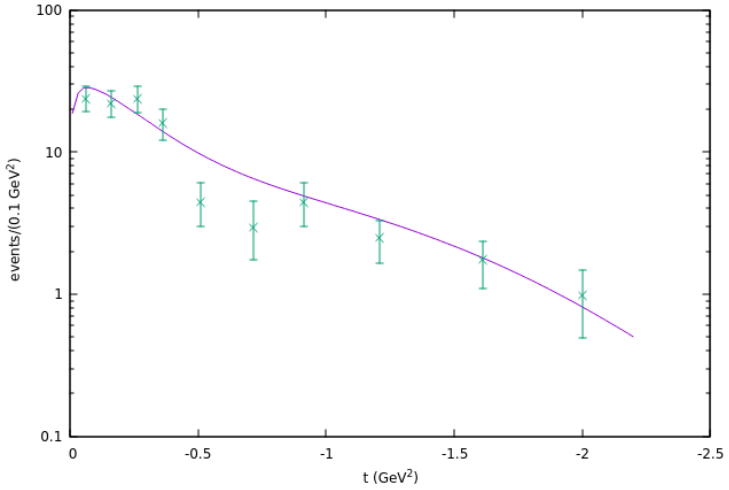


Figure 6.4: Scattering events as a function of $t$, for 4 GeV$^2$ $< W^2 <$ 8 GeV$^2$, with our model compared to data from [43]. The pion Regge propagator is used in the s/u-channel diagram.

propagator again for the axial nucleon channel, as it gave us the best results for the structure function. Using the rho propagator gives largely similar results.

There are 2 graphs from that paper that we will try reproduce with our model. First there is a distribution of events over $W^2$ in the high-energy region, which they define as $W > 2$ GeV. For this, we have to integrate the cross section until it only depends on W and then calculate for increasing W values. We ended up with figure 6.3 and observe that our model does a rather poor job of matching up with the data points. Possibly the influence of the lower $W^2$, where the model works not as well, might distort the curve.

The other graph we reproduce is a similar distribution of events over $t$. To do this we calculate the cross section as a function of $t$ for a number of $Q^2$ and $W$ values and then we average over all these values for each $t$ as an approximation of integrating explicitly over $Q^2$ and $W$. We do this both for lower energies, 2 GeV $< W < 2\sqrt{2}$ GeV and higher energies, $2\sqrt{2}$ GeV $< W <$ 5 GeV (which is a rather arbitrary upper limit). We obtain quite a good fit for the lower energy data and an even better match with the higher energy data, for both models. This is completely in line with earlier results, the higher $W$ region is the region where our model works best.

## 6.2 Neutral Current

For the neutral current the situation is very similar. The diagrams we use are now, due to the Z boson having no charge, the same as we had for electropro-

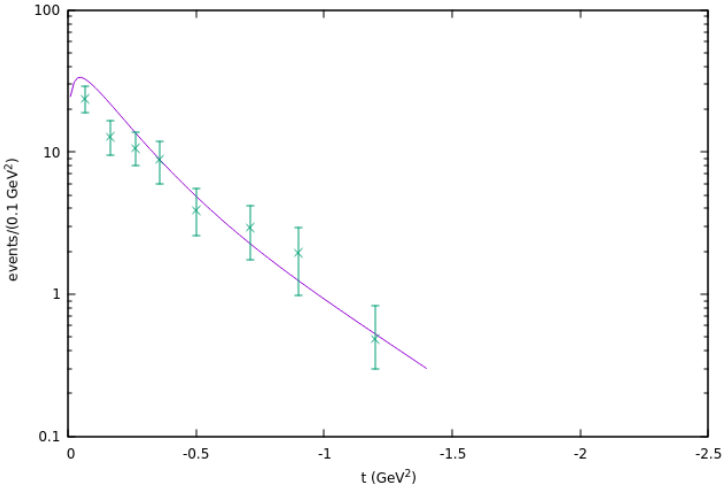


Figure 6.5: Scattering events as a function of $t$, for $W^2 > 8$ GeV$^2$, with our model compared to data from [43]. The pion Regge propagator is used in the s/u-channel diagram.

duction. The isospin is also the same for the weak neutral current diagrams, with the exception of the reactions for which the isospin was zero due to only including the 'electric coupling' (photons not coupling to neutron), as the Z-boson couples to neutrons. In that case we use the same isospin factors for the s- and u-channel terms.

At the vertex level some small changes must be made. In the meson t-channel exchange diagrams we can keep on using the form factors we derived earlier, due to VMD, but now there is an extra factor $(1 - 2\sin^2\theta_W)$ in the $Z\pi x$ vertices. Furthermore we can define the nucleon form factors for Weak NC, derived from the electric form factors through isospin symmetry:

$$F_{s/u}^{Zpp} = \frac{1}{2}(1 - 4\sin^2\theta_W)F_{s/u}^{\gamma pp}$$

$$F_{s/u}^{Znn} = -\frac{1}{2}F_{s/u}^{\gamma pp}$$

where the Weinberg angle $\theta_W$ is given by $\sin^2\theta_W = 1 - (m_W/m_Z)^2$. For the axial form factor we can also derive a relation to the axial form factor in the charged current case:

$$G_A^{nc} = \pm\frac{1}{2}G_A^{cc}$$

where the plus sign is for the proton at the axial vertex and the minus sign for the neutron. For a more in-depth calculation of these neutral current form factors we point to [41] [20].

We cannot do much more with the neutral current pion production model, as there is no available data at the moment.

# Summary and conclusions

The Standard Model of Particle Physics has been the leading theory in particle physics for decades. Its predictive power is not matched by any theory that would try to replace it and through it we have gained a lot of insight into fundamental physics. The Standard Model is not perfect though, there is an area in which the Standard Model failed to match reality: neutrinos. Neutrinos have been observed, in three different flavours, and it was discovered that they can change flavour through a process called neutrino oscillations. This process has been experimentally verified so it is accepted by the physics community, but as a consequence of these oscillations neutrinos got to be massive. This last statement is in direct contrast with the Standard Model, that predicts massless neutrinos. For that reason the field of neutrino oscillations has been one of the most ludicrous areas of research in the last decade.

At this point one of the hurdles for a better understanding of these oscillations is the theory of neutrino-nucleus interactions. To be more precise we lack a neutrino-nucleus cross section that can predict to a high accuracy what happens when a neutrino interacts with a nucleus. Knowledge of this cross section is crucial as neutrino energy (a parameter in neutrino oscillations) can only be reconstructed from a final state and for that reconstruction to be done correctly there needs to be a precise cross section. The part of the neutrino-nucleus cross section that this thesis focuses on is single pion production. SPP is one of the important reaction channels that is lacking a good description. There are a number of working low-energy models, but the focus is on finding an accurate high-energy model.

In this work we try to construct a Reggeized Born term model for high $W$ and low $Q^2$. Regge theory is a theory that expands the often used t-channel particle exchange approach by changing the particle to a Regge trajectory, which consists of a family of particles with increasing spin and mass. Regge theory manages to take these all into account and doing that predicts the $s$-behavior of the cross section, for high $W = \sqrt{s}$. The only unknown that Regge theory does not give to us is the $t$-behavior of the scattering amplitudes. In the Reggeized Born term model that we use this $t$-behavior is taken from the tree-level Feynman diagrams allowed in the particular reaction, the Born terms. This approach has the big advantage that we have no parameters, as all coupling constants in these diagrams have already been measured in other works. The only freedom we have is in choosing the relevant diagrams.

The goal of this model is to get a working description of neutrino-induced pion production, in particular for the neutral current. Because the weak vector current is identical to the electromagnetic vector current, through conserved vector current (CVC), we can start at the electron-induced pion production. As the $Q^2 = 0$ limit of electroproduction is photo-induced pion production, we begin testing our model for photoproduction data.

We have looked at earlier work by Guidal, Laget and Vanderhaegen, and by Kaskulov and Mosel to get the relevant diagrams into our cross section. The results for photoproduction suggest that our model is not ready to be used quantitatively. While it can reproduce the trends of the cross sections in a qualitative correct way, there are still places where the model and the data differ by too much. There are some small changes that we can make to the model and these give us slight improvements. In the charged pion case we have focused most on the different possibilities to scale the variable $s$ in the Regge propagator. For the neutral pion there was also the impact of Regge phase and the question of adding a nucleon exchange diagram. This gave us two distinct neutral pion models for photoproduction that were both able to describe the photoproduction data.

The extension to electroproduction was done by introducing $Q^2$-dependent form factors. These are given to us by vector meson dominance (VMD) for the t-channel diagrams, where we assume that the incident boson behaves like a vector meson at the vertex. In the nucleon channels we also present a form factor to account for propagating nucleons that are highly off-shell and this also prompts the use of a $Q^2$-dependent Regge trajectory in that channel. We have looked at the possibility of adding $t$-dependent coupling constants, as proposed by Vranckx and Ryckebusch, but we rejected that because it worsened our earlier photoproduction results. When comparing to the data we have made a number of changes to the model to see the impact on our predictions. We found that changing the variables in the t-channel form factors had only a limited impact. Changing the off-shell nucleon form factor factor to the simpler Dirac form factor was also considered but we dismissed that on our results for the neutral pion case. The most promising changes were getting rid of the $Q^2$-dependence in the Regge trajectory, which improved our results in all cases, and changing the Regge scale of $s$. In addition the data showed us that one of the two models for neutral pion production we found in the photoproduction case was not sufficient to describe electroproduction.

To go from electroproduction to neutrinoproduction the big challenge was the axial current, as the vector current is the same as the EM vector current by CVC. For the axial current we use a similar property, Partial Conservation of Axial Current (PCAC), to derive the axial currents from the $\pi N$ elastic reaction diagrams. Analogous to the vector current we also introduced axial form factors, both for the rho and nucleon channels. A first comparison between our axial model and data pointed out that the rho channel on its own was not sufficient and an axial nucleon contribution needed to be included in the model. Strange enough we found that the axial nucleon channel with a pion Regge propagator described the data better than a rho Regge propagator, even though that was

not expected. This points out that work on the axial current is far from over. The possibility of adding additional trajectories needs to be researched more throughly. For the total cross section (axial and vector current) in the neutrino case we looked at the few data sets that are available and found in general a good agreement with the data.

We have found a model that describes data from photo-, electro- and neutrino-induced pion production quite good qualitatively, though it needs more work to be quantitatively useful. We have presented some ways in which the model can be amended. For neutrinoproduction processes the data is limited, so a detailed comparison might have to wait and we are convinced that more work on the axial current is crucial. We have constructed a possible way to calculate the weak neutral current SPP from a Regge theoretic framework, and it can be tested with neutral current neutrinoproduction data whenever that is available.

# Samenvatting en conclusies

Het Standaardmodel van de deeltjesfysica is al decennia een breed aanvaarde theory in subatomaire fysica. Het heeft een voorspellende kracht die nog niet geëvenaard is door alternatieve modellen en het heeft ons heel wat inzicht verworven in de fundamentele fysica. Toch is het standaardmodel niet perfect. Op een vlak faalt het Standaardmodel in het beschrijven van de realiteit: neutrinos. Neutrino's zijn in drie verschillende 'smaken' (ook wel generaties) waargenomen en men heeft ondekt dat die neutrino's van smaak kunnen veranderen in een proces genaamd neutrino oscillaties. Dat proces is experimenteel geverifieerd en is geaccepteerd door de fysica gemeenschap, maar een belangrijk gevolg van die neutrino oscillaties is dat neutrino's massief zijn. Massieve neutrino's zijn een directe contradictie van het Standaard Model, dat massaloze neutrino's voorspelt. Daarom zijn neutrino oscillaties momenteel een van de meest actieve onderzoeksgebieden in de deeltjesfysica.

Op dit moment is een van de grootste hindernissen om neutrino oscillaties beter te begrijpen de theorie van neutrino-kern interacties. We missen een neutrino-nucleus cross sectie die heel precies kan berekenen wat er gebeurt wanneer een neutrino interageert met een kern. Kennis van die cross sectie is crucuaal want de neutrino energie (een parameter in neutrino oscillaties) kan enkel gereconstrueerd worden vanuit een finale toestand en om die reconstructie correct uit te voeren hebben we een precieze cross sectie nodig. Het deel van de neutrino-nucleus cross sectie waar deze thesis op focust is 'single pion production' (SPP), het proces waarbij één pion wordt geproduceert door een neutrino-kern interactie. SPP is een van de belangrijke reactiekanalen die nog geen goede beschrijving heeft. Er zijn wel een aantal lage energie modellen, maar momenteel ligt de focus op het vinden van een accuraat hoge energie model.

In dit werk proberen we een gereggeïseerd Born term model te construeren voor hoge $W$ en lage $Q^2$. Regge theorie is een theorie die de veelgebruikte $t$-kanaal deeltjesuitwisseling uitbreidt door het deeltje te veranderen in een Regge traject, wat bestaat uit een familie van deeltjes met stijgende spin en massa. Regge theorie slaagt er in om all die deeltjes in rekening te brengen en voorspelt zo de $s$-afhankelijkheid van de cross sectie voor hoge $W = \sqrt{s}$. De enige onbekende, niet gegeven door Regge theorie, is het $t$-gedrag van de verstrooiingsamplitudes. In het gereggeïseerd Born term model dat wij gebruiken, nemen we het $t$-gedrag uit de laagste orde Feynman diagrammen die toegelaten zijn in de bestudeerde reactie, de Born termen. Het grote voordeel van deze aanpak

is dat we geen vrije parameters hebben, want alle koppelingconstantes in de gebruikte diagrammen zijn al gemeten in andere werken. De enige vrijheid die we hebben is in welke relevante diagrammen we gebruiken.

Het doel van dit model is om een werkende beschrijving van neutrino geïnduceerde pion productie te bekomen, in het bijzonder voor de neutrale stroom. Omdat de zwakke vectorstroom identiek is aan de elektromagnetische vectorstroom, door behoud van vectorstroom, kunnen we eerst elektron geïnduceerde pion productie uitwerken. De $Q^2 = 0$ limiet van electroproductie is foton geïnduceerde pion productie en de eerste stap in deze thesis is om ons model te testen aan fotoproductie data.

We hebben eerder werk door Guidal, Laget en Vanderhaegen, en door Kaskulov en Mosel, bestudeerd om de relevante diagrammen in onze cross sectie te steken. De resultaten voor fotoproductie suggereren dat ons model niet klaar is om gebruikt te worden voor kwantitatieve voorspellingen. Het kan wel degelijk de trends in de cross sectie reproduceren op een kwalitatief correcte manier, maar er zijn toch regio's waar het verschil tussen onze voorspellingen en de data te groot is. Er zijn enkele kleine zaken die we kunnen veranderen aan ons model om de overeenkomst te verbeteren. In het geladen pion geval hebben we ons vooral gefocust op de verschillende mogelijkheden om de parameter $s$ te schalen in de Regge propagator. Voor het neutrale pion is er ook de impact van Regge fase en het eventueel toevoegen van een nucleon uitwisselings diagram. Die laatste geven ons twee neutrale pion modellen, met verschillende diagrammen, die beiden de fotoproductie data kunnen beschrijven.

De uitbreiding naar elektroproductie werd gedaan door $Q^2$-afhankelijke vormfactoren te introduceren. Deze worden gegeven door vector meson dominantie (VMD) voor de $t$-kanaal diagrammen, waarbij we verondersteld hebben dat het inkomende boson zich gedraagt als een vector meson aan de vertex. In de nucleon kanalen gebruiken we een vormfactor om de propagarende nucleonen, die off-shell massa's hebben, in rekening te brengen. Dit doet ons ook een $Q^2$-afhankelijkheid introduceren in de Regge trajecten in het nucleon kanaal. We hebben ook overwogen om $t$-afhankelijke koppelingsconstanten toe te voegen, zoals voorgesteld door Vranckx en Ryckebusch, maar besloten dat toch niet te doen omdat die aanpassing de voorspellingen van ons fotoproductiemodel verslechtert. Bij de vergelijking van ons model met de data hebben we een aantal veranderingen voorgesteld en bekeken wat de impact was op onze voorspelde cross secties. We ondervonden dat het veranderen van de variabelen in de $t$-kanaal vormfactoren slechts een geringe impact heeft. Het wijzigen van de off-shell nucleon vormfactor naar de simpelere Dirac vormfactor is ook overwogen maar verworpen door de tegenvallende resultaten bij neutrale pionen. De meest veelbelovende veranderingen waren het uitschakelen van de $Q^2$-afhankelijkheid in de Regge trajecten, wat onze resultaten in alle gevallen verbeterde, en het veranderen van de Regge schaal van $s$. Verder heeft de data ons ook getoond dat slechts een van de 2 modellen voorgesteld bij neutrale pion photoproductie voldoende was om de electroproductie te beschrijven.

Om van electroproductie naar neutrinoproductie te gaan is de axiale stroom de grote uitdaging, aangezien de vector stroom bepaald is uit de EM stroom via

behoud van vector stroom. Voor de axiale stroom gebruiken we een gelijkaardige eigenschap, partieel behoud van axiale stroom, om de axiale stromen af te leiden uit de $\pi N$ elastische diagrammen. Analoog aan de vectorstroom introduceren we ook axiale vormfactoren, voro zowel de rho als de nucleon kanalen. Een eerste vergelijking tussen ons axiaal model en data toonde dat het rho kanaal op zich niet voldoende was en dat een axiale nucleon contributie nodig was in ons model. Vreemd genoeg merkten we dat een pion Regge propagator in het axiale nucleon kanaal de data beter beschreef dan de rho Regge propagator, ook al was dat helemaal niet wat we verwachtten. Dit maakt het duidelijk voor ons dat het werk aan de axiale stroom verre van voorbij is. De mogelijkheid om aanvullende Regge trajecten toe te voegen moet verder onderzocht worden. Voor de gecombineerde (axiale en vectoriële stromen) cross sectie in het neutrino geval hebben we een vergelijking gemaakt met de weinige data die er is en over het algemeen was de overeenstemming met ons model goed.

We hebben dus een model geconstrueerd dat de data voor foton, elektron en neutrino geïnduceerde SPP goed beschrijft op een kwalitatieve manier, ook al heeft het nog wat werk nodig vooraleer het kwantitatief nuttig kan zijn. We hebben een aantal manieren besproken waarop ons model kan gewijzigd worden. Voor neutrinoproductie processen is de data beperkt, dus een gedetailleerde vergelijking was niet mogelijk, maar we zijn ervan overtuigd dat de axiale stroom nog meer werk nodig heeft. We hebben in deze thesis een mogelijke manier voorgesteld om de zwakke neutrale stroom SPP te beschrijven vanuit een Regge theoretische frame, die kan getest worden vanaf wanneer de eerste neutrale stroom neutrinoproductie data beschikbaar is.

# Wetenschapspopularisatie

Mijn vorm van wetenschapspopularisatie is een filmpje met uitleg over deze thesis voor een breed publiek. Dit is de link naar dat filmpje: https://youtu.be/7IM1mho3FSs.

# Dankwoord

Achter elke thesisstudent schuilt een grote groep mensen die ondersteuning biedt en dat was in mijn geval niet anders. Een schip naar wal loodsen kan enkel als je een goede kaart hebt, dus daarom wil ik allereerst mijn promotoren bedanken: Alexis Nikolakopoulos en Natalie Jachowicz. Alexis zonder jouw mails, meeting calls en uitgebreide uitleg zou deze thesis er niet geweest zijn en was het schip waarschijnlijk nog aan het varen op open zee. Natalie, bedankt voor de vele goede raad (waar ik soms wat beter had naar moeten luisteren), voor de duidelijke instructies en bedankt om af en toe een lach op mijn gezicht te toveren tijdens die vele calls. Ook wil ik graag Jannes Nys bedanken voor de heldere uitleg op de bureau (toen het nog kon). Jan Ryckebusch, ook jij bedankt, want zonder jouw toestemming was heel deze thesis in het Nederlands en dat zou geen verbetering zijn.

Niet iedereen die mij geholpen heeft in deze periode is een fysicus, dus daarom ook een dank aan mijn mama, papa, broer en zus. Jullie zijn er in geslaagd mij genoeg rust te gunnen om dit af te maken en boden het gezelschap wanneer ik daar in deze periode nood aan had. En bedankt om mij van eten te voorzien, dat was ook handig. Ten slotte nog een kleine bedanking aan iedereen tegen wie ik mocht babbelen over neutrino's, o.a. Tristan de Winne (wel een fysicus) en alle leiding van Scouts Windeke (voor zover ik weet geen fysici). Hopelijk hebben jullie er iets van begrepen en zoniet, bedankt om te doen alsof!

# Bibliography


[1] Brown, L. M. (1978). The idea of the neutrino. *Physics Today, 31*(9), 23–28. doi: 10.1063/1.2995181

[2] Chadwick, J. (1914). Intensitätsverteilung im magnetischen Spektren der $\beta$-Strahlen von Radium B + C. *Verhandlungen der Deutschen Physikalischen Gesellschaft, 16* (in German), 383–391.

[3] Zuber, K. (2012). 'Important historical experiments' in*Neutrino physics.* London: Taylor & Francis.

[4] Wilson, F. L. (1968). Fermi's Theory of Beta Decay. *American Journal of Physics, 36*(12), 1150–1160.

[5] Mastbaum, A. T. (2018, April 1). Little, Neutral, Mysterious: An Introduction to Neutrino Physics. Retrieved from https://hep.uchicago.edu/∼mastbaum/compton/pdf/compton87_01-intro_notes.pdf

[6] Cowan, C., Reines, F., Harrison, F., Kruse, H., and Mcguire, A. (1956). Detection of the Free Neutrino: a Confirmation. *Science, 124*(3212), 103–104.

[7] Lande, K. (2018, April 17). Biographical memoirs: Raymond Davis Jr. Retrieved from http://www.nasonline.org/publications/biographical-memoirs/memoir-pdfs/davis-raymond.pdf

[8] Danby, G., Gaillard, J. R., Goulianos, K., Lederman, L. M., Mistry, N. N., Schwartz, M. S., and Steinberger, J. (1962). Observation of High-Energy Neutrino Reactions and the Existence of Two Kinds of Neutrinos. *Physical Review Letters, 9*(1), 36–44.

[9] Perl, M. L., Abrams, G., Boyarski, A., Breidenbach, M., Briggs, D., Bulos, F., Chinowsky, W., Dakin, J., et al. (1975). Evidence for Anomalous Lepton Production in $e^+$ $e^-$ Annihilation. Physical Review Letters, 35(22), 1489.

[10] K. Kodama, et al. (2001). Observation of tau neutrino interactions. *Physics Letters B, 504*(3), 218–224.

[11] Halzen, F., and Martin, A. D. (2016). *Quarks and leptons: an introductory course in modern particle physics.* New York: John Wiley.

[12] Lipari, P. (2001). 'Introduction to Neutrino Physics' in *1st CERN-CLAF School of High-Energy Physics*, 115-199.

[13] Mastbaum, A. T. (2018, April 5). Lost and Found: Solar Neutrinos and Oscillations. Retrieved from https://hep.uchicago.edu/~mastbaum/compton/pdf/compton87_02-solar .pdf

[14] Mesonium and anti-mesonium. *Zh. Eksp. Teor. Fiz. 33*(2), 549–551. February 1957. reproduced and translated in B. Pontecorvo (February 1957). Mesonium and Antimesonium. *Sov. Phys. JETP. 6*(2), 429–431.

[15] M. Tanabashi et al. (2018). Review of Particle Physics. *Physical Review D, 98*(3), 030001

[16] Aguilar, A., Auerbach, L. B., Burman, R. L., Caldwell, D. O., Church, E. D., Cochran, A. K., ... Yellin, S. (2001). Evidence for neutrino oscillations from the observation of $\bar{\nu}e$ appearance in a $\bar{\nu}\mu$ beam. *Physical Review D, 64*(11).

[17] Aguilar-Arevalo, A. A., Brown, B. C., Bugel, L., Cheng, G., Church, E. D., Conrad, J. M., Dharmapalan, R., Djurcic, Z., Finley, D. A., Ford, R., Garcia, F. G., Garvey, G. T., Grange, J., Huelsnitz, W., Ignarra, C., Imlay, R., Johnson, R. A., Karagiorgi, G., ... Katori, T. (2013). Improved Search for $\bar{\nu}\mu \rightarrow \bar{\nu}e$ Oscillations in the MiniBooNE Experiment. *Physical Review Letters, 110*(16).

[18] Alvarez-Ruso, L., Hayato, Y., & Nieves, J. (2014). Progress and open questions in the physics of neutrino cross sections at intermediate energies. *New Journal of Physics, 16*(7), 075015.

[19] Alvarez-Ruso, L. et al. (2018). NuSTEC White Paper: Status and Challenges of Neutrino–nucleus Scattering. *Progress in Particle and Nuclear Physics, 100*, 1–68.

[20] González-Jiménez, R., Jachowicz, N., Niewczas, K., Nys, J., Pandey, V., Cuyck, T. V., & Dessel, N. V. (2017). Electroweak single-pion production off the nucleon: From threshold to high invariant masses. *Physical Review D, 95*(11).

[21] Guidal, M., Laget, J.-M., & Vanderhaeghen, M. (1997). Pion and kaon photoproduction at high energies: forward and intermediate angles. *Nuclear Physics A, 627*(4), 645–678.

[22] Kaskulov, M. M., & Mosel, U. (2010). Deep exclusive charged $\pi$ electroproduction above the resonance region. *Physical Review C, 81*(4).

[23] Kaskulov, M. M. (2011, May 10). Neutral pion electroproduction in $p(e, e'\pi^0)p$ above $\sqrt{s} > 2$ GeV. Retrieved April 5, 2020, from the arXiv database.

[24] Vrancx, T., & Ryckebusch, J. (2014). Charged-pion electroproduction above the resonance region. *Physical Review C, 89*(2).

[25] Itzykson, C., and Zuber, J.-B. (2006). *Quantum field theory.* Mineola, NY: Dover.

[26] Thomson, M. (2013). *Modern Particle Physics.* Cambridge: Cambridge University Press.

[27] Sobczyk, J. E., Hernández, E., Nakamura, S. X., Nieves, J., and Sato, T. (2018). Angular distributions in electroweak pion production off nucleons: Odd parity hadron terms, strong relative phases, and model dependence. *Physical Review D, 98*(7).

[28] Amaldi, E., Fubini, S., & Furlan, G. (1979). *Pion-electroproduction.* Springer-Verlag Berlin Heidelberg.

[29] Donnachie, S. (2005). *Pomeron Physics and QCD.* Cambridge: Cambridge University Press.

[30] Close, F., Donnachie, S., & Shaw, G. (Eds.). (2007). *Electromagnetic Interactions and Hadronic Structure* (Cambridge Monographs on Particle Physics, Nuclear Physics and Cosmology). Cambridge: Cambridge University Press.

[31] Barone, V., and Predazzi, E. (2002). *High-energy particle diffraction.* Berlin: Springer.

[32] Mathieu, V., Fox, G., & Szczepaniak, A. P. (2015). Neutral pion photoproduction in a Regge model. *Physical Review D, 92*(7).

[33] Kamano, H., Nakamura, S. X., Lee, T.-S. H., & Sato, T. (2013). Nucleon resonances within a dynamical coupled-channels model of $\pi$N and $\gamma$N reactions. *Physical Review C, 88*(3).

[34] Boffi, S., Giusti, C., Radici, M., & Pacati, F. D. (1996). *Electromagnetic response of atomic nuclei.* Oxford: Clarendon Press.

[35] Irving, A. C., & Worden, R. P. (1977). *Regge phenomenology.* Amsterdam: North-Holland Publishing Company.

[36] Boyarski, A. M., Bulos, F., Busza, W., Diebold, R., Ecklund, S. D., Fischer, G. E., et al. Richter, B. (1968). 5- to 16-GeV Single-$\pi$ Photoproduction from Hydrogen. *Physical Review Letters, 20*(6), 300–303.

[37] Krusche, B. (2012). Photoproduction of mesons off nuclei. *Progress in Particle and Nuclear Physics, 67*(2), 412–417.

[38] Anderson, R. L., Gustavson, D. B., Johnson, J. R., Overman, I. D., Ritson, D. M., Wiik, B. H., & Worcester, D. (1971). High-Energy $\pi^0$ photoproduction from Hydrogen with Unpolarized and Linearly Polarized Photons. *Physical Review D, 4*(7), 1937–1946.

[39] Park, K., et al. (2013). Deep Exclusive $\pi^+$ Electroproduction off the Proton at CLAS. *The European Physical Journal A, 49*(1), 16.

[40] Bedlinskiy, I. et al. (2014). Exclusive $\pi^0$ electroproduction at $W > 2$ GeV with CLAS. *Physical Review C 90*(2).

[41] Nakamura, S. X., Kamano, H., & Sato, T. (2015). Dynamical coupled-channels model for neutrino-induced meson productions in resonance region. *Physical Review D, 92*(7).

[42] Hernández, E., Nieves, J., & Valverde, M. (2007). Weak pion production off the nucleon. *Physical Review D, 76*(3).

[43] Allen, P., Grässler, H., Schulte, R., Jones, G., et al. (1986). A study of single-meson production in neutrino and antineutrino charged-current interactions on protons. *Nuclear Physics B, 264*, 221–242.

[44] Kamano, H., Nakamura, S. X., Lee, T.-S. H., & Sato, T. (2012). Neutrino-induced forward meson-production reactions in nucleon resonance region. *Physical Review D, 86*(9).

[45] K.A. Olive et al. (Particle Data Group), Chin. Phys. C, 38, 090001 (2014).

[46] Gell-Mann, M., & Lévy, M. (1960). The axial vector current in beta decay. *Il Nuovo Cimento, 16*(4), 705–726.

[47] Mathieu, V., Danilkin, I. V., Fernández-Ramírez, C., Pennington, M. R., Schott, D., Szczepaniak, A. P., & Fox, G. (2015). Toward complete pion nucleon amplitudes. *Physical Review D, 92*(7).